Special Issue

A Review of Adaptive Optics Optical Coherence Tomography: Technical Advances, Scientific Applications, and the Future

Ravi S. Jonnal,[1] Omer P. Kocaoglu,[2] Robert J. Zawadzki,[1] Zhuolin Liu,[2] Donald T. Miller,[2] and John S. Werner[1]

[1]Vision Science and Advanced Retinal Imaging Laboratory, University of California-Davis, Sacramento, California, United States
[2]School of Optometry, Indiana University, Bloomington, Indiana, United States

Correspondence: Ravi S. Jonnal, 4860 Y Street, Suite 2400, Sacramento, CA 95817, USA; rsjonnal@ucdavis.edu.

Submitted: January 8, 2016
Accepted: May 29, 2016

Citation: Jonnal RS, Kocaoglu OP, Zawadzki RJ, Liu Z, Miller DT, Werner JS. A review of adaptive optics optical coherence tomography: technical advances, scientific applications, and the future. *Invest Ophthalmol Vis Sci.* 2016;57:OCT51–OCT68. DOI:10.1167/iovs.16-19103

Purpose. Optical coherence tomography (OCT) has enabled "virtual biopsy" of the living human retina, revolutionizing both basic retina research and clinical practice over the past 25 years. For most of those years, in parallel, adaptive optics (AO) has been used to improve the transverse resolution of ophthalmoscopes to foster in vivo study of the retina at the microscopic level. Here, we review work done over the last 15 years to combine the microscopic transverse resolution of AO with the microscopic axial resolution of OCT, building AO-OCT systems with the highest three-dimensional resolution of any existing retinal imaging modality.

Methods. We surveyed the literature to identify the most influential antecedent work, important milestones in the development of AO-OCT technology, its applications that have yielded new knowledge, research areas into which it may productively expand, and nascent applications that have the potential to grow.

Results. Initial efforts focused on demonstrating three-dimensional resolution. Since then, many improvements have been made in resolution and speed, as well as other enhancements of acquisition and postprocessing techniques. Progress on these fronts has produced numerous discoveries about the anatomy, function, and optical properties of the retina.

Conclusions. Adaptive optics OCT continues to evolve technically and to contribute to our basic and clinical knowledge of the retina. Due to its capacity to reveal cellular and microscopic detail invisible to clinical OCT systems, it is an ideal companion to those instruments and has the demonstrable potential to produce images that can guide the interpretation of clinical findings.

Keywords: adaptive optics, optical coherence tomography, retinal imaging

The 25 years since the advent of optical coherence tomography (OCT)[1] have brought countless improvements in its axial resolution, speed, and sensitivity. The main effort to improve OCT's transverse (or lateral) resolution has been to combine it with adaptive optics (AO), a union that has been investigated in just a few labs. Nevertheless, AO-OCT now plays important roles in the production of knowledge about the retina and its diseases. Chief among these is its potential to resolve ambiguities present in clinical and research-grade conventional (non-AO) OCT systems. Because AO-OCT reveals the microstructure that makes up clinically observable features, it is indispensable as a scientific companion to conventional OCT. Understanding the differences between the OCT image and the AO-OCT image requires that we describe some of the technical details of AO-OCT imaging and image processing, and how these are motivated by the fundamental biological and physical properties of the living human retina.

The Spatial Scale of Retinal Features

The human retina consists of approximately a dozen layers of mostly transparent tissue, together less than half a millimeter thick. The axial resolution afforded by OCT lends itself to imaging the retina's laminar structure. Because retinal diseases often impact this laminar structure, OCT has been used extensively to detect and assess disease and monitor therapeutic efficacy, to such an extent that it has become a standard of ophthalmic care.

Each retinal layer contains structural and functional subunits such as cells, organelles, and capillaries, most of which are too small to be resolved by conventional OCT systems such as the commercial systems employed in the clinic (Fig. 1). While cellular imaging is presently of limited interest to clinicians, it is of great interest to basic science researchers, who stand to learn much about these structures and their functions by imaging them in situ. Moreover, an understanding of the gross structural changes observed in clinical OCT images of disease and recovery depends crucially on knowing their microscopic constituents. Cellular imaging of the retina will continue to expand our understanding of retinal disease, and is therefore of great translational significance.

Optical Factors Affecting Transverse Resolution

The point-spread function (PSF) is a measure of the quality of an imaging system, describing how light originating from a point in tissue manifests in the image of that tissue. The PSF has both

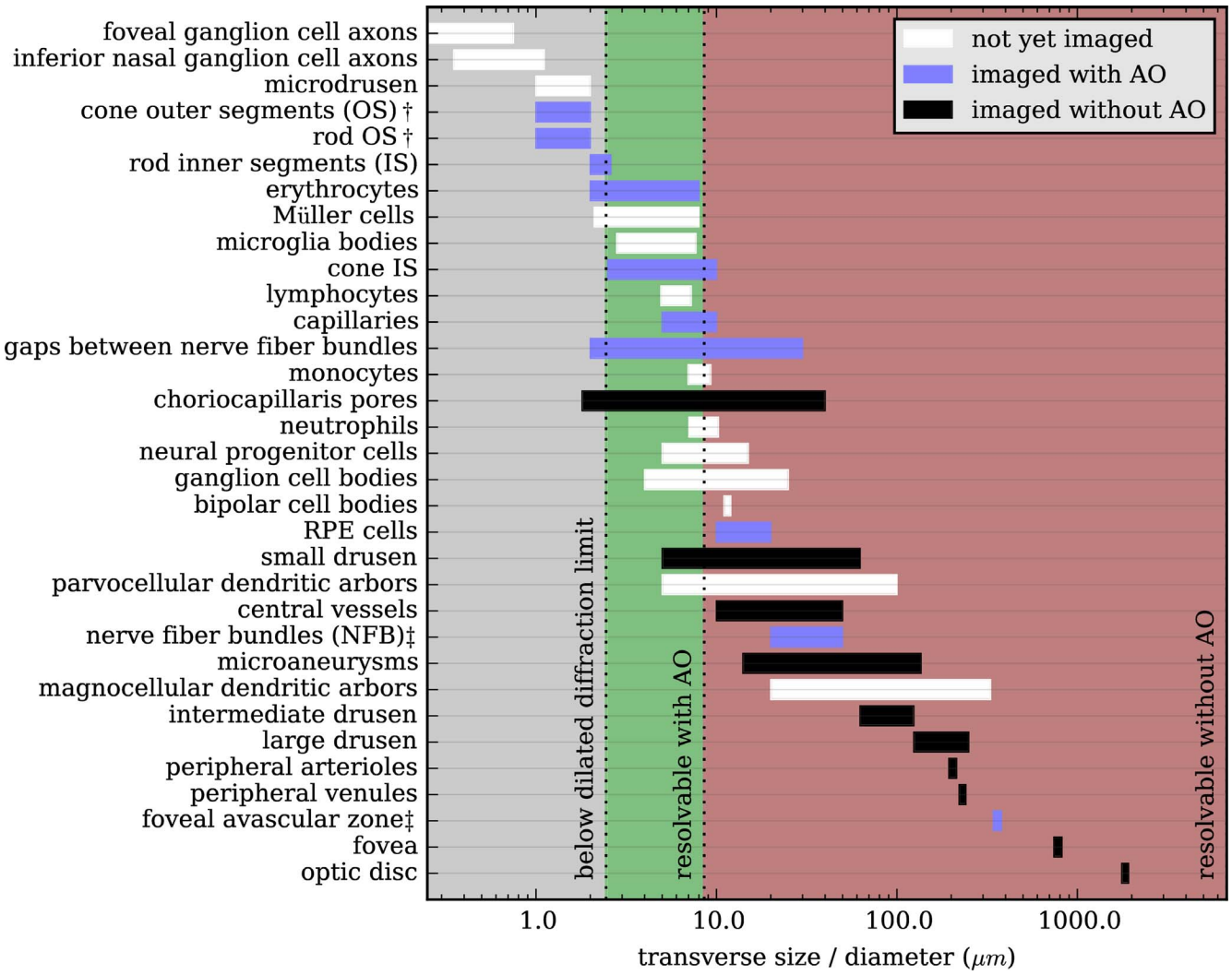

Figure 1. Distribution of transverse size of a small subset of human retinal structures. AO permits visualization of many cellular and subcellular retinal structures. Estimates of sizes are subject to numerous potential sources of error: artifacts of histologic preparation; sampling bias in cases of small numbers of histologic specimens and/or limited sampling across retinal eccentricity; and—where our estimates are based on published micrographs—underestimation of object width due to tangential sectioning of cells. Due to waveguiding, visibility of the cone and rod outer segments (marked with †) is governed by the size of the corresponding inner segments (IS). While the foveal avascular zone‡ and nerve fiber bundles‡ are large, their visibility depends on much smaller features, namely, capillaries and nerve fiber bundle gaps, respectively. Sources: foveal ganglion cell axons[2] ($\mu \pm \sigma$), inferior nasal ganglion cell axons[2] ($\mu \pm \sigma$), microdrusen,[3] cone outer segments (OS)†,[4,5] rod OS†,[5] rod inner segments (IS),[5,6] erythrocytes,[7] Müller cells,[8] cone IS,[9] lymphocytes,[10] gaps between nerve fiber bundles,[11,12] monocytes,[10] choriocapillaris pores,[13,14] neutrophils,[10] neural progenitor cells,[15] ganglion cell bodies[16–18] (with 95% $<$ 13 μm[16]), bipolar cell bodies,[17] RPE cells,[19] small drusen,[20] parvocellular dendritic arbors,[21] nerve fiber bundles (NFB)‡,[11,12] microaneurysms,[22,23] magnocellular dendritic arbors,[21] intermediate drusen,[20] large drusen,[20] peripheral arterioles[24] ($\mu \pm \sigma$), peripheral venules[24] ($\mu \pm \sigma$), foveal avascular zone‡,[25] fovea,[25] optic disc.[26] Resolution limits were computed using $R_x = \frac{1.22\lambda f}{nD}$, assuming an undilated pupil size D of 2.0 mm, a dilated pupil size D of 7.0 mm, an imaging wavelength λ of 840 nm, a bulk refractive index n of 1.33, and an eye length f of 22.2 mm.

transverse (or lateral) and axial components. In an imaging system free of aberrations, transverse resolution is limited by diffraction at the limiting aperture of the system. If the imaging beam is circular with uniform intensity across the pupil, the resulting PSF is an Airy function. Diffraction-limited resolution is defined as the radius of the PSF's first Airy disk zero, also termed the Rayleigh criterion.

The human eye, as an optical system, is fundamentally limited by two factors: first, aberrations intrinsic to the cornea and crystalline lens, and second, diffraction due to the finite size of the eye's pupil. Monochromatic aberrations of the eye vary over the pupil[27,28] and increase monotonically with pupil size. Thus with a dilated pupil, resolution is limited by aberrations ("seeing limited") rather than the finite pupil ("diffraction limited"). To achieve optimum resolution across a larger pupil (>6 mm), correction of higher-order aberration is necessary. As shown in Figure 1, diffraction-limited imaging through a large pupil theoretically allows visualization of many features of interest in the living human retina.

Resolution, however, is not the only factor affecting visibility. Strict criteria such as the Rayleigh criterion do not take account of the variations in contrast among the features of interest, relative to the imaging system's noise. The amount of light reflected or scattered from these features, however, varies considerably. These variations may explain why some structures theoretically resolvable conventionally (e.g., ganglion cell bodies) and with AO (e.g., bipolar cell bodies) have yet to be imaged in vivo (Fig. 1). Methods to increase the contrast of

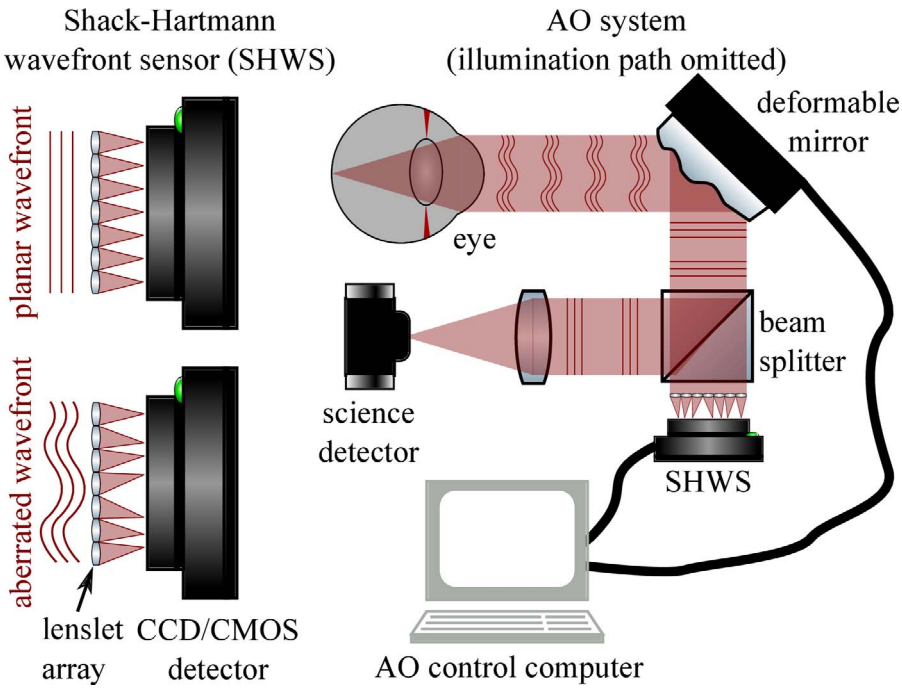

Figure 2. The concepts of Shack-Hartmann wavefront sensing (SHWS) and closed-loop AO correction with a deformable mirror. A SHWS works by sampling a wavefront with an array of small lenses (lenslets) such that local wavefront slope—due to aberration—manifests as displacement of the resulting focal spot (*left*). These displacements can be used directly to drive a corrector such as a deformable mirror (*right*), or to reconstruct the wavefront by Zernike polynomial fitting, for example.

retinal images (e.g., motion correction and averaging, spectroscopic OCT, polarization-sensitive OCT, angiographic algorithms, contrast agents, and darkfield and phase-contrast techniques) remain areas of active investigation.

Improving Transverse Resolution With Adaptive Optics

Diffraction-limited imaging is achieved by measuring and correcting ocular monochromatic aberrations over a dilated pupil. These are most commonly implemented with a Shack-Hartmann wavefront sensor and deformable mirror, respectively (Fig. 2), yielding unprecedented transverse resolution (2–3 μm), sufficient for resolving individual cells in the living human retina.[29]

While the diffraction-limited PSF summarizes the static performance of an AO system, the aberrations of the living human eye change over time. Thus the temporal bandwidth of

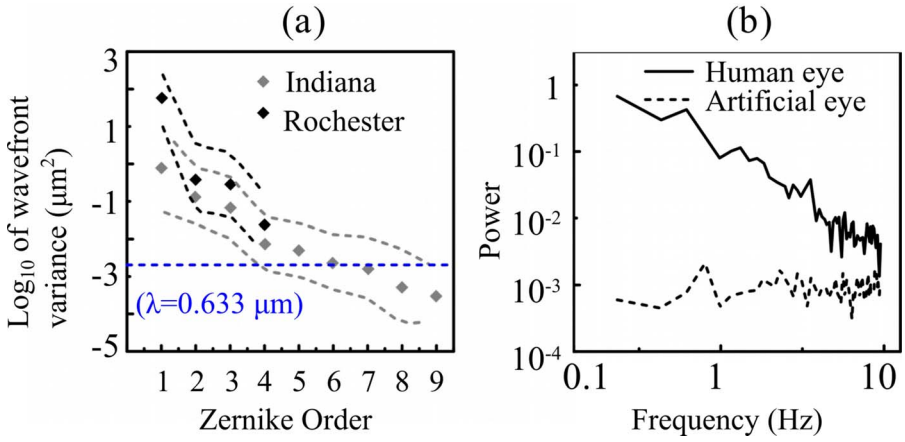

Figure 3. Spatial and temporal power spectra of ocular aberrations. (**a**) The power of aberrations, measured as variance in wavefront height over the dilated (7.5 mm) pupil, declines with increasing spatial frequency (here expressed in terms of Zernike order).[28] At 633 nm, the diffraction-limited wavefront root mean square (RMS) can be estimated (by the Maréchal criterion of $\lambda/14$) to be 0.045 μm RMS, or a log_{10} (*var*) of −2.7. The observed aberrations drop below this level at about the seventh Zernike order, corresponding to the first 28 Zernike terms. *Diamonds* and corresponding *dashed curves* represent the mean and mean ± 2 standard deviations of the log_{10} (*var*), respectively, for 70 eyes. (**b**) The temporal power spectra of aberrations in a human eye and artificial eye.[30] The power of ocular aberrations falls to 10% of the peak power around 1 Hz. *Left image* reprinted with permission from Doble N, Miller DT, Yoon G, Williams DR. Requirements for discrete actuator and segmented wavefront correctors for aberration compensation in two large populations of human eyes. *Appl Optics*. 2007;46:4501–4514. © 2007 Optical Society of America. *Right image* reprinted with permission from Hofer H, Artal P, Singer B, Aragón JL, Williams DR. Dynamics of the eye's wave aberration. *J Opt Soc Am A*. 2001;18:497–506. © 2001 Optical Society of America.

Investigative Ophthalmology & Visual Science

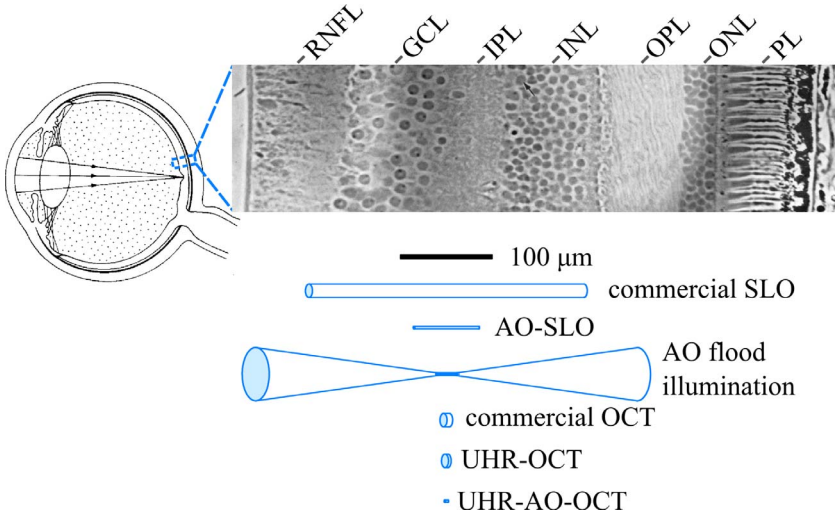

FIGURE 4. Comparison of cell size in a histologic cross section of the human retina with the resolving capability of the major types of retinal imaging modalities with and without AO. The width and length of the blue cylinders and bicone denote the transverse and axial resolutions of the instruments. Examples shown include commercial SLO, AO-SLO, AO flood illumination, commercial OCT, UHR-OCT, and UHR-AO-OCT. GCL, ganglion cell layer; IPL, inner plexiform layer; INL, inner nuclear layer; OPL, outer plexiform layer; ONL, outer nuclear layer; PL, photoreceptor layer; RNFL, retinal nerve fiber layer. The histologic cross section is from Boycott BB, Dowling JE, Kolb H. Organization of the primate retina: light microscopy. *Philos Trans R Soc Lond B*. 1969;255:109–184, © 1969, by permission of the Royal Society.

the AO system (governed largely by the AO correction rate, controller gain, and delays in the loop) affects image quality. Initial estimates of the bandwidth of ocular aberrations were 1 to 2 Hz (Fig. 3, right), suggesting that a loop rate between 10 and 40 corrections per second would cancel them (assuming typical latencies and gain) and achieve closed-loop performance near the diffraction limit (Strehl ratio > 0.8).[30] Later, aberration bandwidths of 30 Hz[31–33] or higher[34] were observed, suggesting that substantially higher rates may be beneficial. A recent study using a rate of 110 corrections per second demonstrated the predicted improvements in resolution and contrast.[33]

Separate from improved transverse resolution, AO improves other aspects of OCT imaging. Adaptive optics reduces the average width of speckle, thereby improving visibility of features larger than the resolution limit. By permitting imaging through a large pupil, AO also increases the amount of light collected from the retina, improving sensitivity and SNR.[35,36]

The majority of ophthalmic AO studies to date have been conducted with two-dimensional (2D) modalities such as flood-illumination and scanning light ophthalmoscopy (SLO). For reviews of these see Williams[37] and Carroll et al.[38] The present review is limited to AO-OCT studies.

The Promise of Three-Dimensional Cellular Imaging

For cellular imaging, high axial and transverse resolutions are necessary. Optical coherence tomography by itself provides the necessary axial resolution but needs AO to achieve the necessary transverse resolution. Figure 4 illustrates the advantage of AO, comparing the size of the three-dimensional (3D) resolution in tissue for commercial OCT, ultrahigh-resolution (UHR) OCT, and AO-equipped UHR-OCT, along with that of commercial SLO and AO-SLO for comparison. As shown, the addition of AO to commercial OCT and UHR-OCT improves their resolution volume by 36 times and achieves a resolution voxel smaller than most retinal cells.

The first implementations of AO-OCT were based on time-domain OCT (TD-OCT), which was the main OCT approach prior to 2004. These implementations included a flood-illuminated version using an areal charge-coupled device (CCD) camera[39] and a conventional version using tomographic (xz) scanning.[40,41] These first instruments demonstrated the potential of the combined technologies to image the living human retina, but fundamental technical limits, primarily in speed, impeded their scientific and clinical use. Nevertheless they represented first steps toward more practical designs that became possible with new OCT methods.

In 2004, new techniques began to supplant TD-OCT in research settings, with clinics following suit within a few years. The main shift was toward frequency-domain OCT, a class of OCT techniques in which detection takes place in the domain of spatial frequency instead of space, namely spectrometer-based spectral-domain OCT (SD-OCT) and swept-source OCT (SS-OCT). These technologies are described extensively in other papers in this special issue.

The axial resolution (the thickness of the PSF) in OCT is determined by the spectral properties of the imaging source.[42] Shorter wavelengths and broader spectral bandwidths result in better resolution, but these are practically limited by the comfort and safety of human subjects and chromatic aberrations.

Development of AO-OCT for In Vivo Human Imaging

Achieving Three-Dimensional Cellular Resolution

In 2005, two studies demonstrated the feasibility of in vivo, 3D cellular resolution imaging. Zhang et al.[43] used a broadband source to illuminate a line on the retina, revealing cone photoreceptors resolved transversely and axially. Soon after, Zawadzki et al.[44] developed a system that raster scanned a point source across the retina, acquiring one spectrum at a time. This system, which also produced cellular-resolution images, would become a template for successive AO-SD-OCT systems, which employ X-Y scanning and detection with a linear spectrometer. Zhang et al.[45] followed their parallel detection scheme by developing an X-Y raster scanning system, but with a 512-pixel spectrometer having an A-line

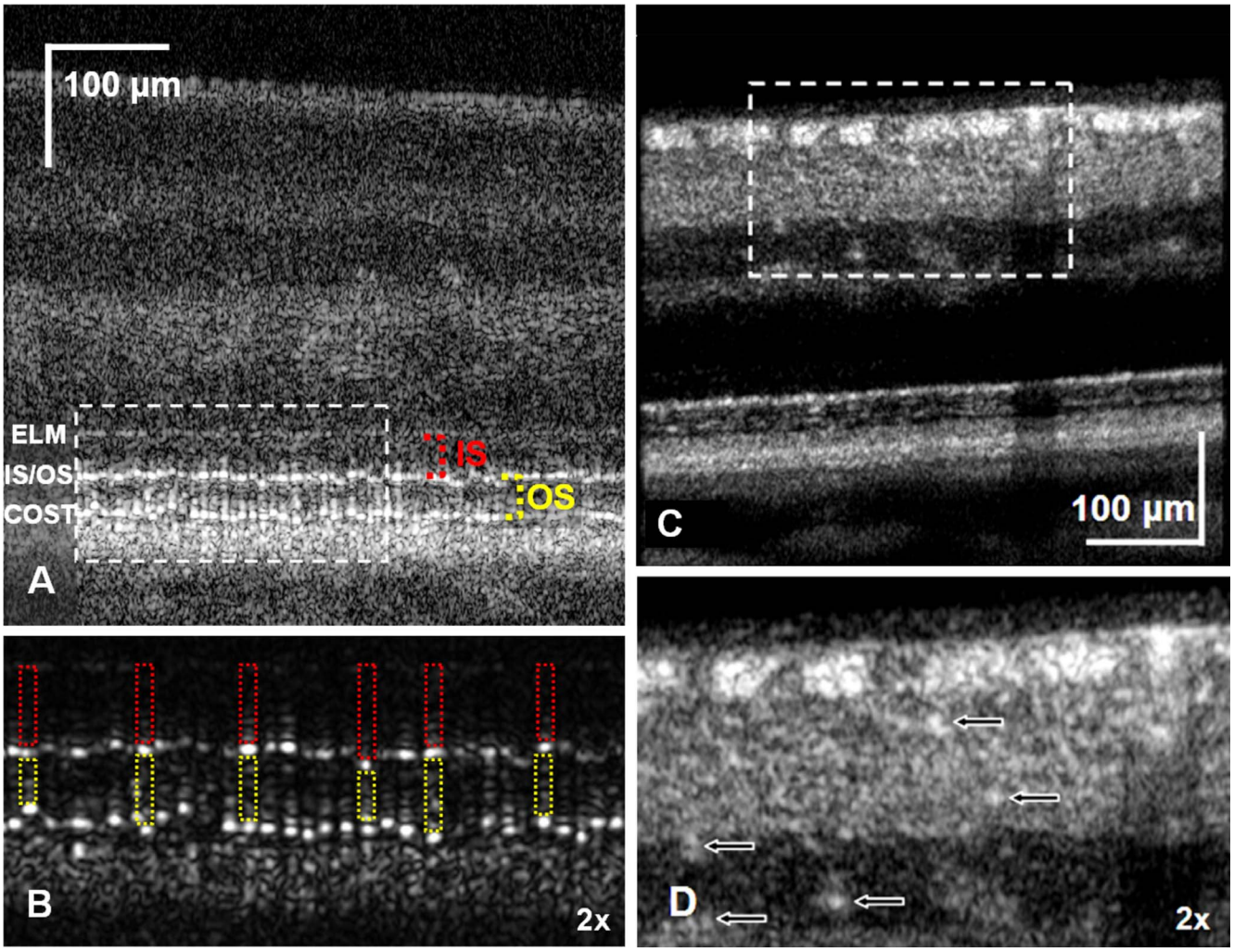

FIGURE 5. Images acquired with AO ultrahigh-resolution OCT. In a log-scale B-scan focused on the outer retina, the ELM, IS/OS, and COST bands are clearly visible, demarcating the IS and OS of the cones. In a linear-scale, magnified view (*bottom left*), the IS/OS and COST reflections from individual cones are clearly visible, with *red and yellow boxes* outlining the relatively transparent individual inner and outer segments. The width of the bright reflections is consistent with known IS widths, while their height is comparable to the axial PSF height, which suggests origination at thin reflectors. Axial displacement of neighboring reflectors is apparent in both layers. When focus is shifted to the inner retina, individual nerve fiber bundles, up to 50 µm in diameter but separated as little as 5 µm, become visible. A magnified view of the latter (*lower right*) reveals capillaries (*arrows*) lying in multiple plexuses. These individual structures of the inner and outer retina appear as uniform bands in clinical OCT images.

rate of 75,000 Hz. They imaged retinal patches sufficiently small (150 × 38 µm) to mitigate most eye movement artifacts, acquiring volumes at a rate of 13 Hz and permitting 3D visualization of cellular and other microscopic structures.

Improvements in Bandwidth, Resolution, and Speed

Improvements in axial resolution have made possible insights into the laminar structure of the retina. Because the axial dimension of the PSF in OCT is inversely proportional to the bandwidth of the imaging source, investigators sought ways to increase these bandwidths. Broadband sources (>100 nm) were available, but their utility was limited by the impact of longitudinal chromatic aberration (LCA), which would thwart the benefits of AO. Zawadzki et al.[46] and Fernandez et al.[47] implemented broadband sources by developing custom achromatizing lenses to induce complementary LCA in the incoming beam, such that all wavelengths of the incoming beam would focus at equal depth in the retina. The system designed by Zawadzki et al. employed a broadband superluminescent diode (SLD) source ($\Delta\lambda = 112$ nm, $\lambda = 836$ nm) and achieved an isotropic 3D resolution of 3.5 × 3.5 × 3.5 µm in the eye. The resulting improved image quality (Fig. 5) marked the advent of AO ultrahigh-resolution OCT (AO-UHR-OCT).

At the same time, attempts were made to improve further the systems' transverse resolution. In the first few years of active AO-OCT research, AO systems were built around microelectrical–mechanical systems (MEMS) and other low-stroke mirrors that lacked sufficient range of motion to correct the dominant ocular aberrations of defocus and astigmatism. Two studies[48,49] addressed this issue by implementing a woofer–tweeter AO architecture with two mirrors: a high-stroke bimorph mirror with relatively few actuators, designed to compensate the eye's low-order aberrations; and a low-stroke MEMS mirror with more actuators, designed to compensate high-order aberrations. Zhang et al.[45] improved wavefront correction by repositioning the deformable mirror close to the eye. Evans et al.[50] in 2009 performed an error budget analysis, resulting in further improvement in transverse resolution. Mujat et al.[51] used a woofer–tweeter AO system

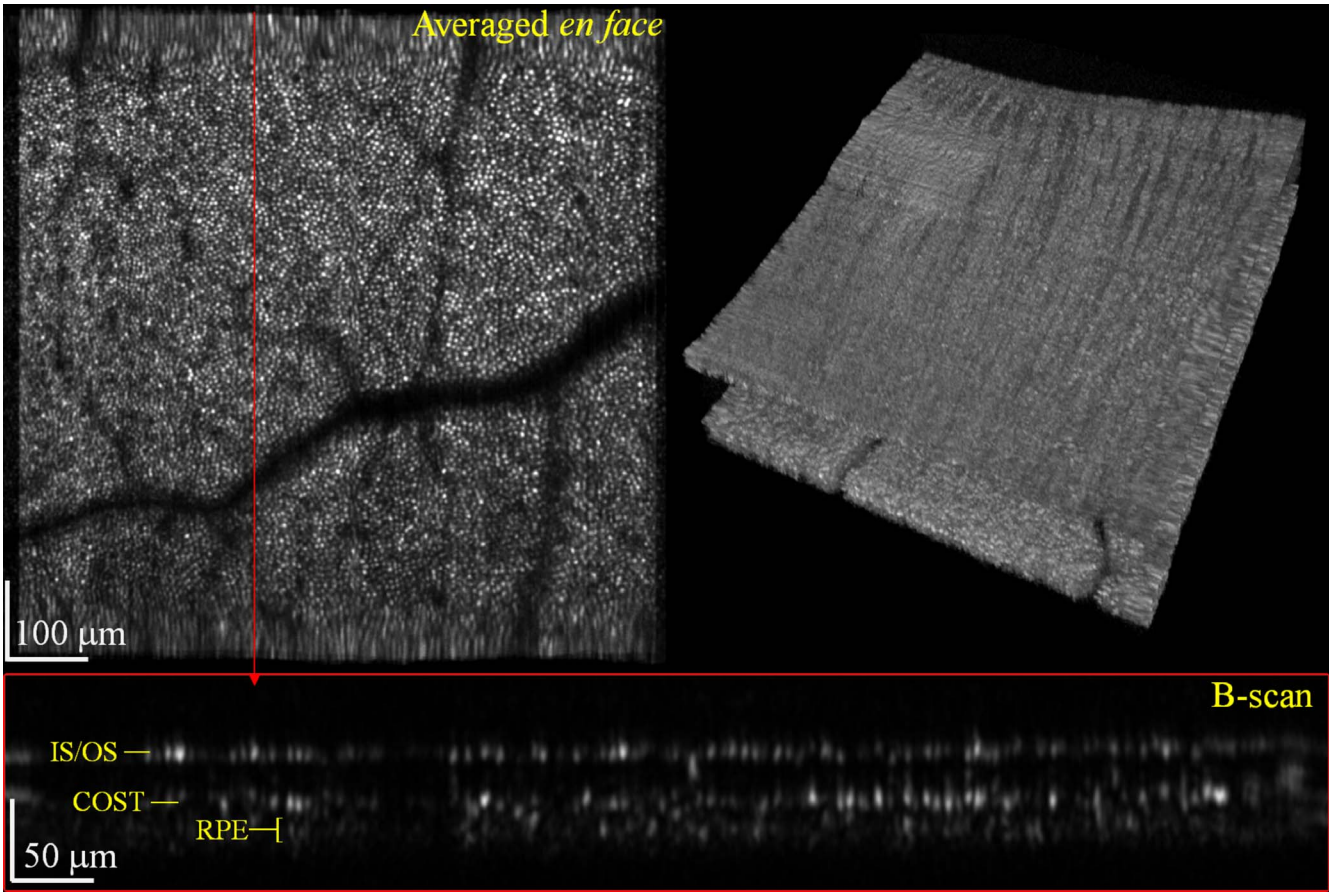

FIGURE 6. AO-OCT images acquired at an unprecedented 1-MHz line rate. Three-dimensional projection of volumetric image (*top right*) shows very small amount of axial eye motion with good preservation of the laminar retinal structure. The en face view of the photoreceptors (*left*) shows cones resolved clearly throughout the image without averaging, with quality comparable to that of AO-SLO images of the same, but in 3D. The linear-scale B-scan (*bottom right*) shows the axial detail present at each column of pixels in the en face view, sufficient to show the cone OS and RPE reflections. Reprinted with permission from Kocaoglu OP, Turner TL, Liu Z, Miller DT. Adaptive optics optical coherence tomography at 1 MHz. *Biomed Opt Express*. 2014;5:4186–4200. © 2014 Optical Society of America.

combined with a SS-OCT ($\lambda = 1$ μm) in order to image deeper into the retina. Inspired by approaches in the AO-SLO community to correct aberrations and distortions generated by spherical-mirror telescopes used in most AO systems,[52,53] two AO-OCT groups deployed novel strategies for doing the same. Lee et al.[54] devised an out-of-plane design while Liu et al.[55] developed an in-the-plane one based on custom toroidal mirrors.

One of the major limitations of AO-OCT systems is the presence of eye motion artifacts. This effect is similar to motion artifacts present in standard retinal imaging systems; however, higher magnification offered by AO-OCT and the fineness of the observable structures increase the impact of eye movements. Thus there has been a consistent push to improve the speed of AO-OCT systems. Torti et al.[56] employed a faster spectrometer, acquiring 120,000 A-lines/second, producing 3D images of the retina with notably fewer eye motion artifacts. Many investigators soon followed suit,[12,36,54] and some employed active retinal tracking as an additional means of reducing motion artifacts.[57]

Pircher et al.[58] adopted a novel approach to the problem of motion artifacts by developing a high-speed, time-domain, scanning AO-OCT system. This system acquired 2D en face images of the retina at various depths, at speeds similar to those with AO-SLO. As such, artifacts in single frames were further reduced.

Kocaoglu et al.[59] achieved an order-of-magnitude improvement in speed by implementing a quadplexing spectrometer design capable of recording 1 million A-scans per second. This system was, at the time, the fastest retinal SD-OCT system reported, with or without AO. It permitted imaging of a large field of view with minimal motion artifacts and, because it employed aberration-canceling toroidal mirrors, maintained optimal transverse resolution. The resulting images (Fig. 6) represent some of the most promising AO-OCT images to date, revealing artifact-free microscopic detail at many layers in the retina.

Enhancing AO-OCT for Measuring Biological Properties of the Living Retina

Over the last decade several attempts have been made to tailor AO-OCT to the measurement of the unique structural and functional aspects of the living human eye. These efforts mainly included incorporation of complementary imaging modalities, automated segmentation of retinal structures, removal of artifacts created by involuntary eye movement, and expansions of OCT detection schemes to functional imaging.

Combining AO-OCT With AO-SLO. One area of AO-OCT development is its combination with AO-SLO.[58,60–62] Adaptive optics SLO provides a complementary view of retinal structures and additionally allows detection of fluorescence

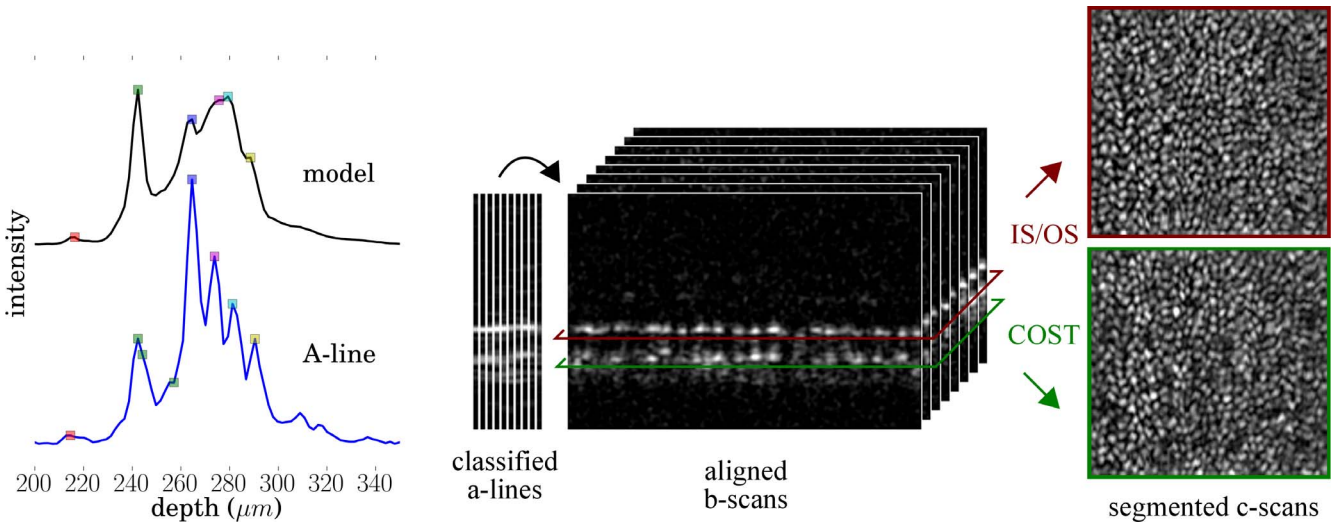

FIGURE 7. Model-based segmentation of AO-OCT A-lines. First, a model of retinal reflectance is generated by aligning and averaging together all of the A-lines in the volume. The resulting model represents the main reflective surfaces of the retina, but lacks much of the high-frequency variation due to speckle and other sources of noise. Each A-line in the volume is then labeled by correlation with the labeled model (*left*). The labels are then used to project layers of interest (*right*).

signals and multiply scattered photons, both invisible to OCT. Moreover, AO-SLO can be used as a tool to detect and correct eye movements during AO-OCT data acquisition.[63]

Automated Three-Dimensional Segmentation. Automated segmentation of the OCT image is an important component of research-grade and commercial instruments, providing objective assessment of changes in retinal layer thickness and enabling various kinds of computer-aided diagnostics. Improvements in layer visibility afforded by SD-OCT motivated advanced segmentation algorithms based on support-vector machines,[64,65] graph-theoretic optimization,[66–69] Markov boundary models,[70] adaptive thresholding and binarization,[71] kernel-based optimization,[72] and RPE segmentation using polarization-sensitive OCT and depolarization detection.[73] Many of the optimization algorithms penalized contour roughness to avoid spurious segmentation of speckles, thereby emphasizing the laminar structure of the retina.

Several of the retinal layers that appear smooth and continuous in conventional OCT images were revealed by AO-OCT to consist of discrete, discontinuous, and axially displaced structures. In conventional OCT images, the retinal nerve fiber layer (RNFL) appears to be a homogeneous, hyperreflective band, whereas AO-OCT reveals the individual nerve fiber bundles that constitute it.[12,49,74] Similarly, while the smooth appearance of the cone inner–outer segment junction (IS/OS) and cone outer segment tip (COST) bands in conventional images is useful for modeling outer retinal morphology,[70] AO reveals these layers to be rough and discontinuous.[75,76] For automated segmentation of the rough IS/OS and COST layers, Jonnal et al.[77] devised a model-based approach. Each A-line in the volume is correlated with a labeled model of gross local retinal reflectance in order to automatically locate and label features in the A-line that correspond with the model's labels. Pixels labeled with a feature of interest (e.g., IS/OS or RPE) can then be assembled into an en face view of that feature (Fig. 7).

Motion Estimation and Correction. Each point in the OCT raster scan requires either spatial or temporal resolution (in SD-OCT and SS-OCT, respectively) of the spectral dimension, both of which require more time than the single photodetector measurement required by SLO, and lead to comparably larger eye motion artifacts in the resulting images.

Techniques for estimating and correcting eye motion artifacts are attractive to OCT researchers for several reasons. Spectral-domain OCT requires partially coherent sources of illumination, a necessary consequence of which is the presence of speckle noise. While speckle noise is deterministic, it becomes uncorrelated over time such that averaging successive images of the same tissue can reduce its impact. However, OCT volumes of the living human retina cannot be averaged without first removing motion artifacts. Moreover, serial imaging of the retina—required for both monitoring retinal disease and functional imaging—necessitates motion correction in order to repeatedly locate the structure of interest over time.

Initial efforts utilized manual alignment, allowing multiple volumes to be stitched together into montages and effectively improving the system's field of view.[78] Automated axial and lateral alignment of B-scans within volumes was applied to improve en face visualization of retinal layers,[45,49] and such en face projections were further corrected using thin-plate spline dewarping.[36] Using segmented projections of IS/OS and COST, Jonnal et al.[77] adapted a strip-based registration method (Fig. 8) developed in the AO-SLO community.[79] This approach was used to track single cones over hours in order to observe outer segment renewal[77] and to assess test–retest reliability of cone morphometry.[75]

Phase-Sensitive AO-OCT for Functional Cellular Imaging. Functional AO-OCT has the potential to combine probes of function (and dysfunction) offered by electrophysiological techniques with the cellular resolution afforded by AO-OCT. One such approach is phase-sensitive AO-OCT, which has the capacity to measure cellular function at a scale of tens of nanometers, 100 times smaller than OCT's axial resolution.

A reflective surface in the retina causes constant-frequency modulation of the k (wave number) spectrum. Fourier transformation of the resulting fringe yields the depth of the surface, but with precision S_z limited spectral range interrogated by the spectrometer $[\lambda_1, \lambda_N]$, with $S_z = \left[\frac{2n}{\lambda_1} - \frac{2n}{\lambda_N}\right]^{-1}$. For a typical UHR-SD-OCT system, with $\lambda_1 = 755$ nm and $\lambda_N = 913$ nm, the resulting axial localization precision is 1.85 μm in the retina. This value is designed to be close to the axial resolution of the system, as reflectors spaced more closely than the resolution cannot be disambiguated with additional precision.

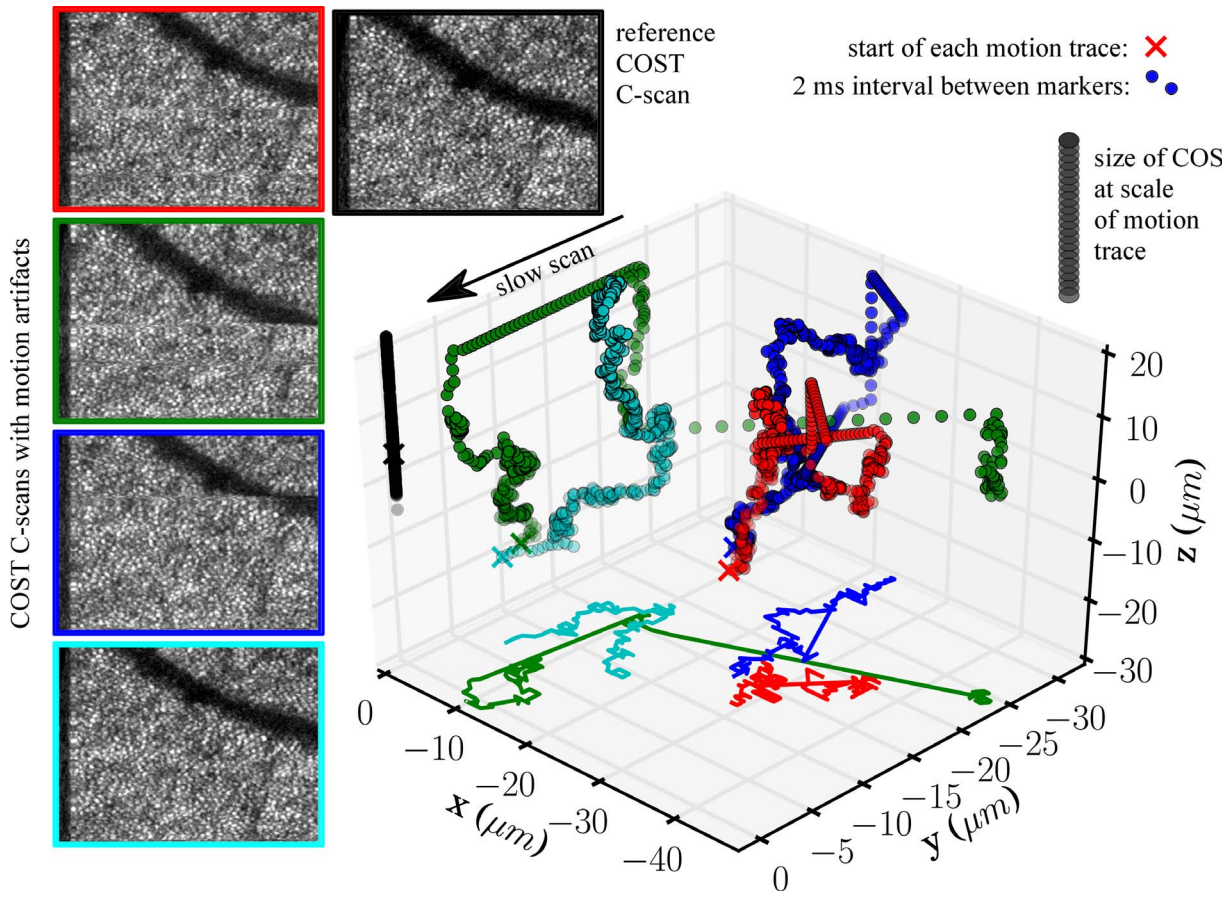

Figure 8. Strip-based motion estimation from AO-OCT volumes. The COST layer was segmented from each of five volumes, four targets to be registered (*left*) and one to be used as a reference frame (*top*). Each target frame was divided into numerous thin strips, along the fast (*horizontal*) dimension, which were then cross-correlated with the reference frame. The resulting cross-correlation peaks, along with segmented depths, provide an X-Y-Z motion trace of the retina (*bottom right*). The volume marked in *green* contains artifacts of multiple fast, saccadic movements, evident in the en face projection and the motion trace plot. Axial motion can be observed in a single volume, but lateral motion only by comparison with a reference volume; thus the black (reference) trace depicts only axial motion. A single cone OS is smaller than the magnitude, in all dimensions, of eye movements, which highlights the need for motion correction in AO-OCT.

For some applications, however, such as attempts to measure axial motion of single reflective objects, isolated in depth,[36,80] this may not be an important consideration. Where there is no need to distinguish among closely spaced reflectors, improving localization precision may be beneficial without attendant increases in axial resolution.

The Fourier transformation of the k spectrum gives both the amplitude of modulation at each frequency (related to the intensity of reflection at the corresponding depth) and the phase of the modulation. Deflections smaller than S_z of retinal structures may cause no observable change in the intensity image while dramatically affecting the phase. This property of OCT was initially exploited in microscopy to visualize subresolution motion of chick embryonic cardiomyocytes.[81]

Generally, this approach is not suitable for in vivo human imaging because gross motion of the eye (Fig. 8, eye motion trace) can result in relatively large phase changes that bury the microscopic changes one is seeking to observe. Phase differences between pairs of reflectors in the retina, however, are immune to such burial, since the phase of both reflections is affected identically by gross motion of the eye. Jonnal et al.[77] exploited this property to detect elongation of the cone OS due to disc renewal.

Improving the Fidelity of Retinal Images With Spectral Shaping. Meadway et al.[62] investigated two methods for digitally modifying AO-OCT spectra prior to Fourier transformation in order to reduce artifacts in the resulting axial PSF. In the first, they multiplied the acquired spectra by a Gaussian window. This approach reduced intensity in the tails of the spectrum, where unsuppressed peaks lead to PSF sidelobes. In the second, they derived a shaping function, such that multiplication with the acquired spectra resulted in a Gaussian shape. These two approaches (or a combination of them) were shown to substantially improve the axial resolution of the system, as well as modestly improve the system's signal to noise ratio (SNR). Qualitatively, the resulting B-scans were notably free of PSF artifacts, and structures of interest were more easily visible (Fig. 9).

Scientific Applications of AO-OCT

Visualizing Microscopic Anatomy of the Retina In Vivo

Adaptive optics OCT has been used to study the three-dimensional microscopic anatomy of the living human retina (see Fig. 10). An immediate impact of this work has been in aiding interpretation of clinical (non-AO) OCT images. The clinical proliferation of OCT systems has revolutionized our understanding of many retinal diseases, but the limited transverse resolution of those systems impedes an understand-

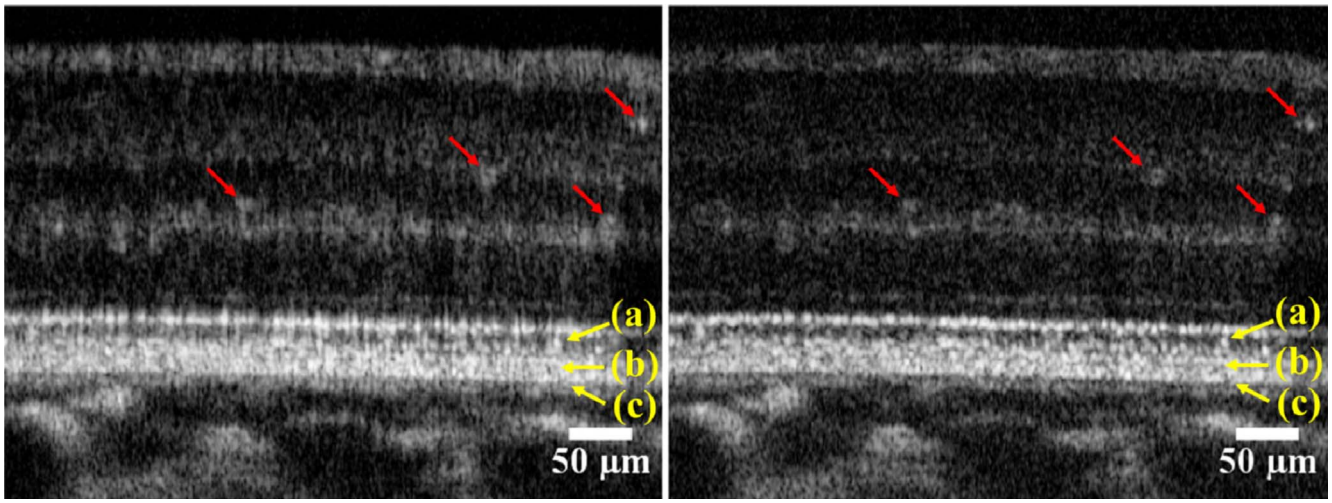

FIGURE 9. Spectral shaping improves image quality in AO-OCT images. Artifacts in the axial PSF, due to the non-Gaussian shape of the imaging source's spectrum, manifest as axial smear and/or ringing in the AO-OCT B-scan (*left*). Application of spectral shaping techniques[62] removes these artifacts (*right*), improving definition of isolated structures like capillaries (*arrows*) and individuation of superjacent layers such as IS/OS (**a**), COST (**b**), and Bruch's membrane (**c**). Reprinted with permission from Meadway A, Girkin CA, Zhang Y. A dual-modal retinal imaging system with adaptive optics. *Opt Express*. 2013;21:29792–29807. © 2013 Optical Society of America.

ing of the cellular changes observed in disease. Adaptive optics OCT does not yet have an appreciable presence in the clinic, but by imaging the same structures with microscopic resolution, has the demonstrated capability of aiding interpretation of clinical images.

Visualization of the Cone Outer Segment Tips. As previously described, Zhang et al.[45] minimized motion artifacts by imaging small patches of retina at high-volume acquisition rates. The resulting volumes permitted en face projections of retinal layers, and revealed that the third outer retinal band, previously considered to originate from the RPE, consisted of two partially overlapping bands with greatly different en face appearance (see Fig. 11). The more proximal of the two bore resemblance (and high statistical correlation) with the IS/OS layer, while the more distal did not. The former was hypothetically attributed to the COST, while the latter's attribution to RPE was maintained.

The Anatomic Origins of Retinal Bands. While attributions of outer retinal bands 1 and 4 to the external limiting membrane (ELM) and RPE have been broadly accepted by the research and clinical communities,[82] the origins of bands 2 and 3 have been controversial, with a number of investigators attributing them to the inner segment ellipsoid (ISe)[82–84] and interdigitation zone (IZ)[83] between the RPE microvilli and outer segments. Jonnal et al.[75,76] used AO-OCT to quantitatively investigate band 2 morphology and concluded that the ellipsoid does not generate band 2, on the two bases that the band was too narrow by a factor of 4 and too distant from the ELM. Figure 12 shows a comparison between a clinical (Spectralis) image of band 2 and an AO-OCT image of band 2, clearly illustrating the improved ability of the latter to perform cellular, morphometric analysis.

Photoreceptor Function

Renewal of outer segment discs is a cellular process critical for the well-being of photoreceptors, and failure of this process may be implicated in some retinal diseases such as AMD. Jonnal et al.[85] measured renewal with AO coherent flood illumination, effectively using the outer segment as an interferometer. The resulting modulation of intensity, over the course of hours, was hypothesized to originate from elongation of the cone OS and associated phase changes between IS/OS and COST. The observed frequencies of modulation corresponded to renewal rates between 99 and 113 nm/hour. A weakness of this approach was the inability to axially localize the source of the interference effects. While OCT can determine the axial locus of a reflector, the complementary processes of renewal and shedding are confined to an axial range comparable to the resolution of UHR-OCT.

Pircher et al.[80] identified a subset of cones exhibiting an extra reflection between the IS/OS and COST reflections. The origin of these reflections is not known but is presumed to be stationary relative to neighboring discs. Unlike COST, whose total range of movement is limited by disc shedding to a few microns, these reflections migrate down the OS. The authors capitalized on this feature to measure OS renewal in a significant subset of the cones to have a mean rate of 110 nm/hour (Fig. 13).

Jonnal et al.[77] later showed that phase-sensitive AO-OCT could be used to detect changes in OS length of 40 nm, two orders of magnitude smaller than the system's axial resolution. They applied this method to measure the rate of renewal at COST, regardless of whether the cone contained extra reflectors, and found that cones at 1.5° eccentricity elongated at rates of approximately 150 nm/hour, roughly consistent with previous measurements,[80,85] while suggesting possible eccentricity-dependent (Jonnal RS, et al. *IOVS* 2010;51:ARVO E-Abstract 2933) or diurnal[85] variation in renewal rate.

Optical Properties of Photoreceptors

Most AO studies of cone pathology have focused on cone loss, but AO-OCT offers the possibility of observing changes in the cone's waveguiding properties, which may precede outright loss. Recently Liu et al.[86] tested the hypothesis that cones' modal properties may manifest as modulation of their transverse intensity profile by using AO-OCT to image the 3D reflectance profile of individual cones at the IS/OS and COST locations. As illustrated in Figure 14, they found that the two cone segments waveguide light differently depending on retinal location. With this baseline, it is now possible to determine whether changes in these modes might be linked to the underlying cone health.

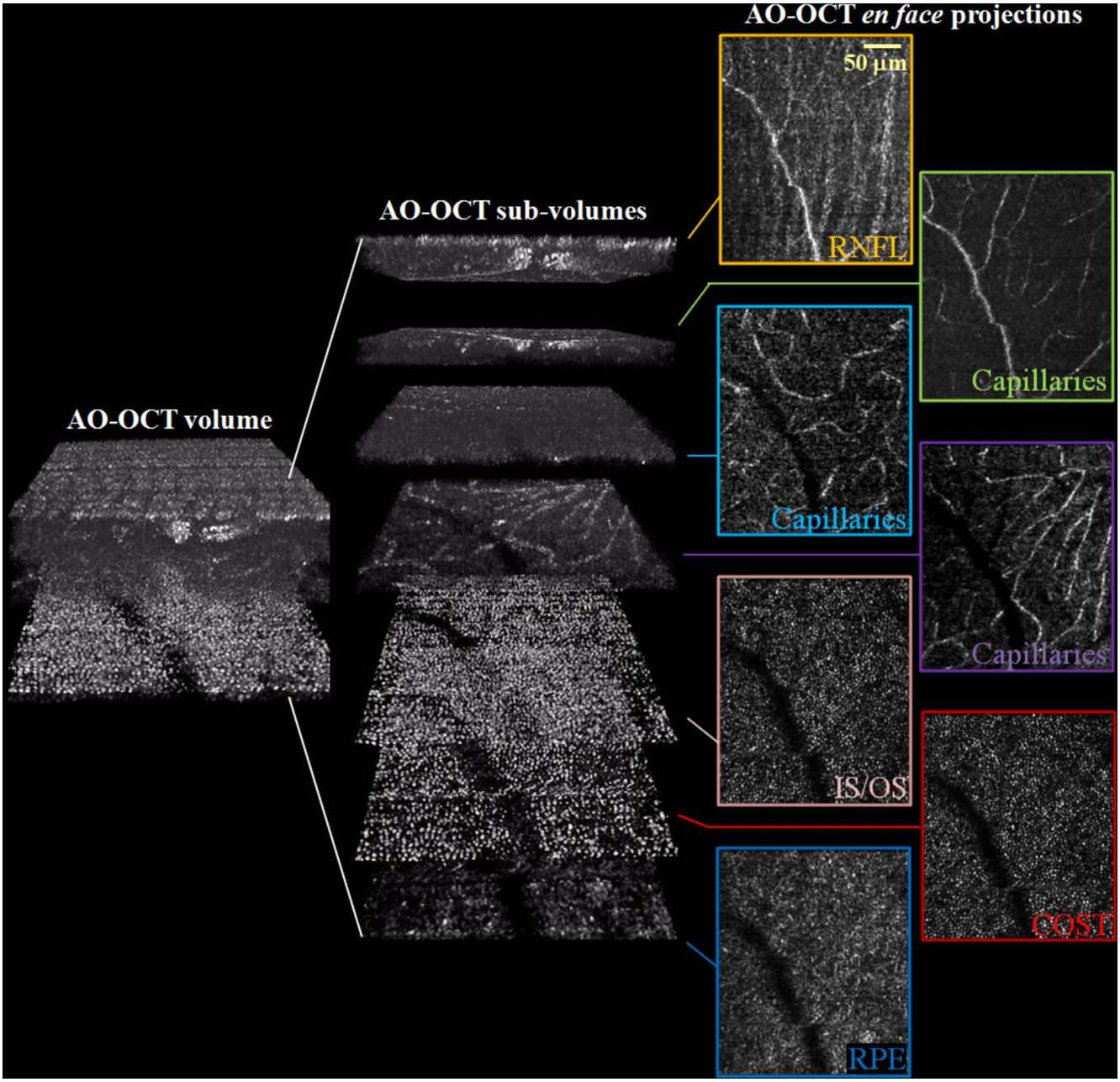

FIGURE 10. Linear-scale AO-OCT volume acquired with three different AO focus depths (RNFL, OPL, and IS/OS) and combined for displaying appearance of retinal layers in AO-OCT images. En face images are projections of subvolumes shown in the *middle*, demonstrating the fine-depth sectioning ability of AO-OCT.

Applications of AO-OCT in Imaging Retinal Disease

Age-Related Macular Degeneration. With AO-OCT it is possible to identify subcellular photoreceptor structures and structural changes not visible in clinical images (Figs. 5, 10). Panorgias et al.[87] used AO-OCT to study geographic atrophy (GA). Losses in IS/OS reflectivity were observed in three of four cases in areas that retained underlying RPE. At the GA margin, visual function persisted even though the IS/OS lost reflectivity, a paradox echoed by recent AO-SLO investigations of macular telangiectasia.[88] This loss of reflectivity may be due to disorganization of the cones and reduced efficiency in light coupling, as was also suggested by Zhang et al.[89] in areas around subretinal drusenoid deposits. Panorgias et al.[87] showed that cone numbers in the GA margin were underestimated without consideration of the optical Stiles-Crawford effect, attesting to the importance of functional measurements in buttressing the observations with structural imaging. Methods developed to characterize morphologic changes in photoreceptors could be applied to other degenerative diseases of the retina, such as Stargardt's disease, retinitis pigmentosa, and cone/rod or rod/cone dystrophies.

Glaucoma and Other Optic Neuropathies. The possibility of outer retinal changes in glaucoma and other optic neuropathies has been investigated using postmortem techniques, with equivocal results.[90–92] This possibility has not, however, been investigated extensively with in vivo imaging methods. Adaptive optics OCT length measurements of the photoreceptor IS and OS of glaucoma patients, however, reveal

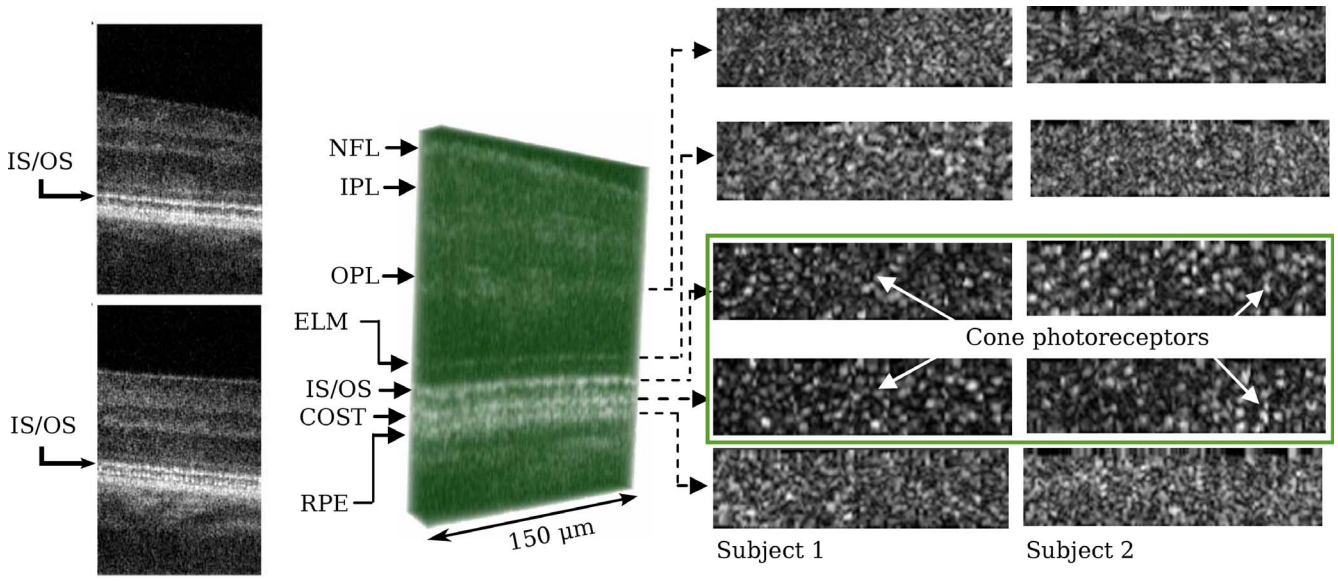

Figure 11. AO-OCT images of the cones and observation of the cone outer segment tips (COST). The IS/OS of individual cones was first observed in AO-OCT B-scans.[43,44] Representative B-scans from 2° (*top left*) and 4° (*bottom left*) are shown. Higher-speed acquisition[45] permitted visualization of small volumes (*center*) and en face projections of layers, some of which were similar to previous AO images of the cone mosaic. High degrees of visual similarity and statistical correlation between the cone-like projections suggested a common cellular origin, while significant axial displacement (≈30 μm) implicated the proximal and distal boundaries of the outer segment, that is, IS/OS and COST, consistent with light microscopy. *Left* reprinted with permission from Zawadzki RJ, Jones SM, Olivier SS, et al. Adaptive-optics optical coherence tomography for high-resolution and high-speed 3D retinal in vivo imaging. *Opt Express*. 2005;13:8532–8546. © 2005 Optical Society of America. *Center* and *right* reprinted with permission from Zhang Y, Cense B, Rha J, et al. High-speed volumetric imaging of cone photoreceptors with adaptive optics spectral-domain optical coherence tomography. *Opt Express*. 2006;14:4380–4394. © 2006 Optical Society of America.

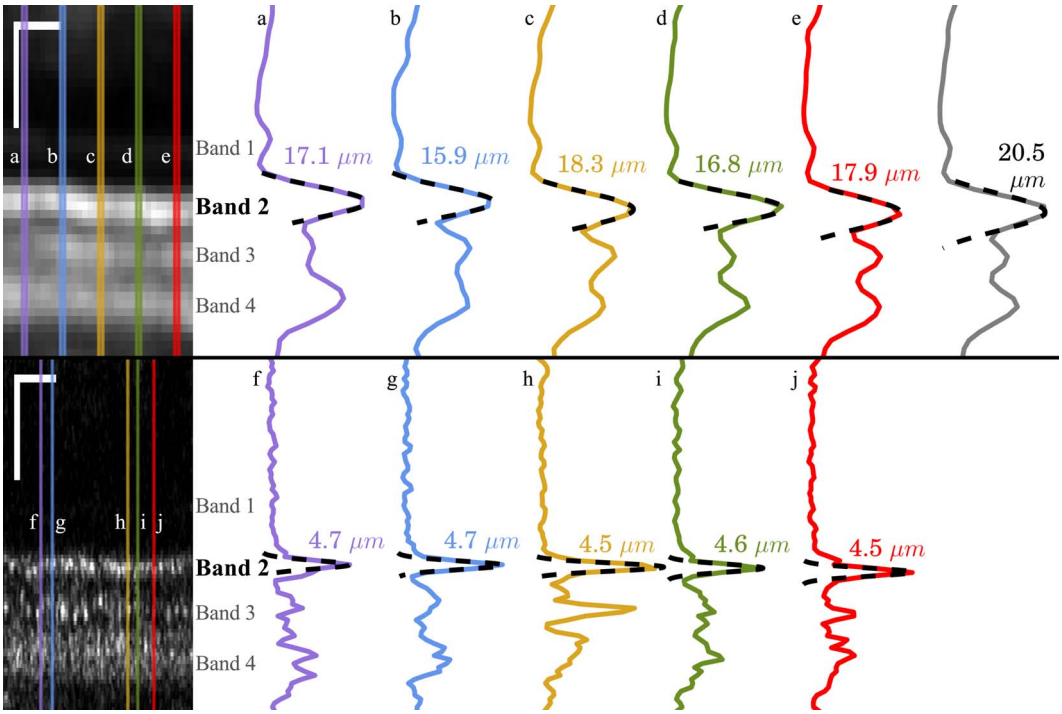

Figure 12. OCT band 2 is narrow when resolved in single cells. A 210-μm-wide section of a Spectralis B-scan (*top left*), acquired at 5.0° and converted to linear intensity scale. The *overlaid lines* indicate the locations of the five A-scans plotted at *top right*. The sixth (*gray*) plot represents the average of 10 A-scans (56 μm). Overlaid on each plot is a least-squares Gaussian fit (*dashed line*), from which the width of the peak can be calculated, as indicated for each A-scan. A comparable linear-scale AO-OCT B-scan (*bottom left*) from the same subject and eccentricity, and plotted A-scans (*bottom right*) selected by identifying bright cones in the image. Widths measured with AO-OCT were considerably smaller, which suggests that axial displacements of IS/OS among neighboring cells, combined with optical blur, cause the band to appear broader than it should in conventional OCT images. *Scale bars*: 50 μm. Reprinted with permission from Jonnal RS, Kocaoglu OP, Zawadzki RJ, Lee S-H, Werner JS, Miller DT. The cellular origins of the outer retinal bands in optical coherence tomography images. *Invest Ophthalmol Vis Sci*. 2014;55:7904–7918. © 2014 The Association for Research in Vision and Ophthalmology, Inc.

Investigative Ophthalmology & Visual Science

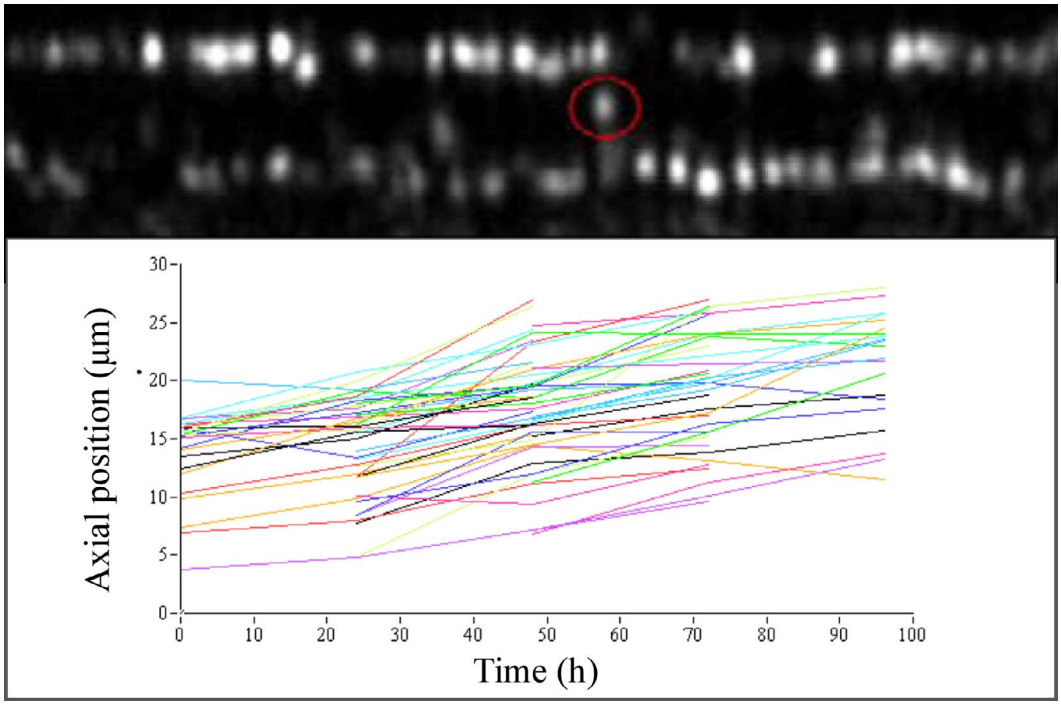

Figure 13. In vivo measurement of outer segment renewal. AO-OCT cross-sectional images (*top*) of a small minority of cones reveal extra reflections between IS/OS and COST (*red circle*).[80] Pircher et al. capitalized on these features to measure outer segment renewal in the living human retina. The axial locations of these spots, plotted against time (*bottom*), show a mean OS renewal rate of 110 nm/hour, consistent with animal studies and AO flood illumination.[85] Reprinted with permission from Pircher M, Kroisamer JS, Felberer F, Sattmann H, Götzinger E, Hitzenberger CK. Temporal changes of human cone photoreceptors observed in vivo with SLO/OCT. *Biomed Opt Express*. 2011;2:100–112. © 2010 Optical Society of America.

a reduction in cone photoreceptor density and outer segment length[93] in areas of expected thinning of the RNFL. In patients with longstanding optic neuropathies, losses in the photoreceptor layers occur as well.[94]

Most glaucoma research focuses on the inner retina, usually employing gross measures of RNFL thickness. As shown in Figure 5, it is possible to visualize bundles of optic nerve fibers with AO-OCT, presumably because the gaps between bundles are smaller than the resolution afforded by clinical OCT (Fig. 1). These individual bundles were first demonstrated by Zawadzki et al.[49] and later by Cense et al.[74] and Torti et al.[56] Kocaoglu et al.[12] demonstrated lost bundles in a patient with a well-defined arcuate scotoma. In each case, AO-OCT provided a unique opportunity to characterize the 3D morphology of individual bundles.

Polarization-sensitive OCT (PS-OCT)[95] demonstrates that glaucoma affects the polarization properties of RNFL before thinning is observed with standard OCT. Cense et al.[35] incorporated polarization-sensitive detection with AO-OCT (AO-PS-OCT) and demonstrated an improvement in the

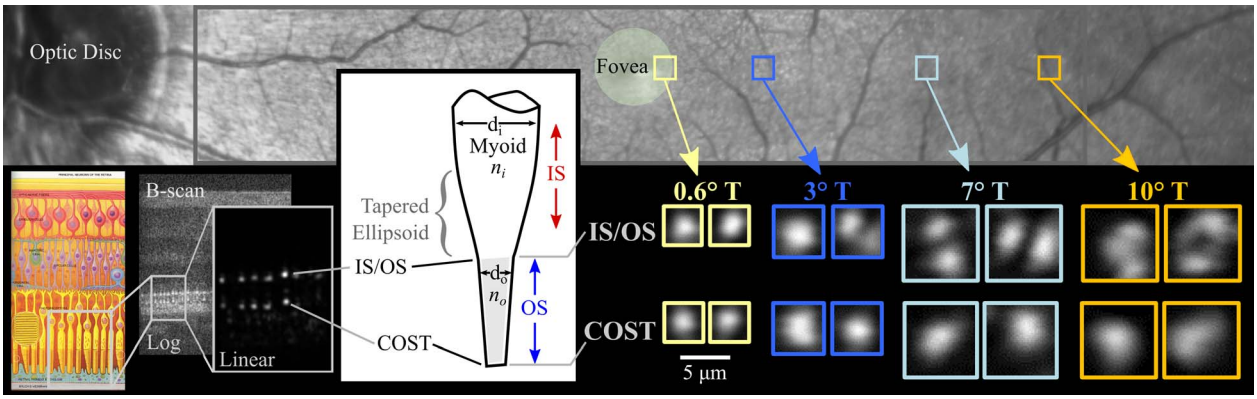

Figure 14. Evidence of differences in modal content between inner and outer segments. AO-OCT images of the cones were collected at four retinal eccentricities (*top*), over which the IS diameter varies between approximately 2 and 10 μm but the OS diameter does not vary appreciably. After segmenting the IS/OS and COST reflections from individual cones (*bottom, second from left*), en face projections of both structures can be visualized as a function of IS diameter (*bottom right*). The intensity distribution at IS/OS changes with eccentricity, becoming bimodal between 3° and 7° and more multimodal at 10°, suggesting that outer segments and narrow inner segments behave like single-mode fibers and wider inner segments like multimode fibers. Diagram of retinal neurons (*lower left*) reprinted with permission from Aramant RB, Seiler MJ. Retinal transplantation. *Sci Med*. 2000;7(1):20–29. © 2000 Science and Medicine.

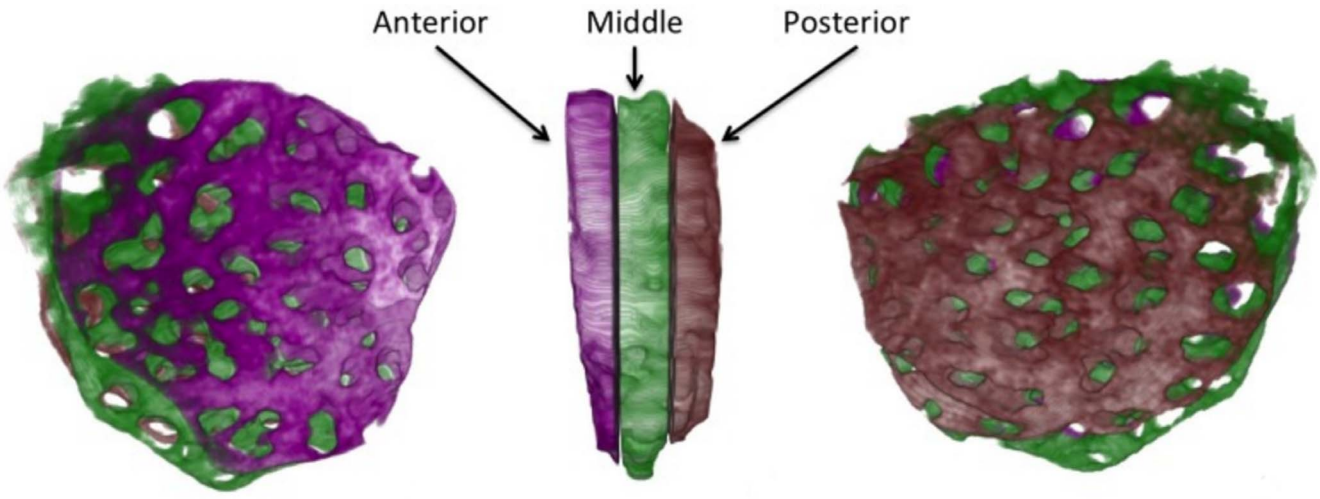

FIGURE 15. The porous structure of lamina cribrosa revealed with AO-OCT. Monitoring changes in the structure of lamina cribrosa may have important clinical applications, because such changes are thought to be associated with elevations in interocular pressure associated with glaucoma. Torti et al.[56] and Nadler et al.[96] (shown above) have applied AO-OCT to deep imaging of the lamina cribrosa, revealing its porous structure in microscopic detail. Combined with automated techniques for measuring the pores and other aspects of the structure, this approach may yield insight about glaucoma progression. Reprinted with permission from Nadler Z, Wang B, Schuman JS, et al. In vivo three-dimensional characterization of the healthy human lamina cribrosa with adaptive optics spectral-domain optical coherence tomography. *Invest Ophthalmol Vis Sci*. 2014;55:6459–6466. © 2014 The Association for Research in Vision and Ophthalmology, Inc.

reliability of polarization measurements due to the improved SNR of AO-OCT.

In addition to quantifying inner and outer retinal changes in glaucoma, it is also important to image the lamina cribosa (LC), the multilayered porous network buried in the optic nerve head through which ganglion cell axons and major blood vessels must pass. Strain in the LC from elevated intraocular pressure may cause loss of axoplasmic flow associated with glaucomatous loss of ganglion cells. Imaging portions of LC has been possible at high volumetric resolution with AO-OCT,[56] with resulting 3D images showing its detailed porous structure[96] (Fig. 15), and promises to be a valuable tool for early diagnosis and assessment of glaucoma. Because LC is substantially deeper than the neural retina, it can be more effectively imaged by extending the depth range of the OCT, such as by complex conjugate removal techniques.[97]

Diabetic Retinopathy. Two-dimensional AO images have been used to quantitatively characterize lumens of diabetes-affected retinal capillaries[98] and to classify retinal microaneurysms.[23] Optical coherence tomography provides a 3D view of these structures, and visibility of microvasculature and blood flow has been demonstrated using AO-OCT–based systems.[49,99–101] The 3D views of such microscopic structures afforded by AO-OCT may offer additional power to AO-based diagnostics, especially if combined with OCT angiography or flow measurement. Such applications may further improve diagnosis of mild diabetic retinopathy before the onset of more severe sequelae (such as edema and neovascular proliferation) that are commonly used to diagnose the disease.

Stem Cell Treatment for Degenerative Disorders of the Retina. Park et al.[102] used AO-OCT to monitor the efficacy of intravitreal stem cell injections in treating a patient with Stargardt's disease. Clear differences were visible between baseline images and images acquired 1 month after injection. An array of hyperreflective spots was visible in AO-OCT images of the inner retina, but not visible with OCT alone. The size of these spots was consistent with the injected CD34+ cells, suggesting that the cells had migrated from the vitreous into the neural retina.

THE FUTURE OF AO-OCT

Functional Imaging of Stimulus-Evoked Changes in Photoreceptors

Two sorts of stimulus-evoked optical changes have been observed in photoreceptors. First, stimulus-evoked changes in near-infrared scattering ("intrinsic signals") have been characterized extensively in vitro. These have also been measured using in vitro OCT,[103] in vivo OCT,[104,105] and AO-SLO.[106] Adaptive optics OCT offers a way to measure the same changes, but with 3D cellular resolution. Second, stimulus-evoked changes in the outer segment's optical length have been observed.[107] These changes may be of greater interest because the time scale over which they occur agrees with the known time scale of phototransduction; they are initiated within a few milliseconds of a stimulus and progress rapidly over the first 30 to 50 ms. Phase-sensitive AO-OCT, which provides resolution of OS length changes two orders of magnitude smaller than the OCT axial resolution,[77] may permit study of these stimulus-evoked changes.

Functional Imaging of RPE

Retinal pigment epithelium cells play a central role in supporting and maintaining photoreceptors. While dysfunction of the RPE underlies numerous retinal pathologies, biomarkers sensitive to RPE change at the cellular level are limited. Recently AO-OCT in combination with subcellular registration and a novel contrast agent (organelle motility) has been used successfully to visualize and characterize the 3D morphology of RPE cells and their packing geometry.[108] But even more sensitive biomarkers may be possible that are linked to cellular physiology. New efforts are under way to correlate RPE organelle motility with RPE function using AO-OCT as the tool to detect these motion-evoked changes in the scatter of light (Liu Z, et al. *IOVS* 2016;57:ARVO E-Abstract 2807).

OCT Contrast Agents

One of the major limitations of OCT is its inability to detect fluorescent signals. This greatly limits cellular and molecular specificity as well as functional applications of OCT systems. There are several efforts to overcome this limitation by application of OCT-specific contrast agents. Existing examples include nanoparticles such as gold cages[109] and microspheres[110] along with complex detection schemes (pump probe OCT[111] and photothermal OCT[112,113]). Future application of AO-OCT will surely benefit from any advance made in this field.

AO-OCT Angiography

Recent developments in OCT angiography (OCTA) methods (see Gorczynska et al.[114] for a thorough comparative analysis) have demonstrated improved visualization of retinal, and especially choroidal, vasculature. As retinal capillaries and the pores of the choriocapillaris, especially in the fovea, lie at the resolution limit for conventional imaging systems (Fig. 1), both would benefit from the application of AO, especially because early disease-related changes in their morphology are likely to be even smaller. Such an approach could have great basic scientific and translational value in investigations of diseases such as AMD and diabetic retinopathy, as well as in acute retinal conditions such as artery and vein occlusions. Initial results in this area are encouraging (Kurokawa K, et al. *IOVS* 2016;57:ARVO E-Abstract 5915).

Computational AO-OCT

Within a few years of the first AO images of the retina,[29] investigators recognized that computational methods could be used to deblur retinal images, either with or without information about the ocular wave aberrations causing the blur. Early efforts employed blind deconvolution[115,116] as well as wavefront sensing,[117,118] the corresponding PSF of which was used as a deconvolution kernel.

Recently, an alternative to deconvolution has been suggested, in which the object structure is reconstructed by solving sets of inverse scattering problems.[119] Other groups have applied a virtual Shack-Hartmann wavefront sensor (SHWS) to estimates of the distribution of light in the pupil plane based on the OCT image.[120]

Computational approaches to improving spatial resolution are attractive for numerous reasons: They obviate deformable mirrors, substantially reducing the cost and complexity of imaging systems and improving clinical deployability; they have the capacity to provide depth-invariant aberration correction by optimizing image quality independently for each depth in the sample; and they offer anisoplanatic imaging possibilities, where the complement of aberrations may vary significantly across the lateral extent of the sample.

On the other hand, algorithms for computational AO-OCT are highly sensitive to noise in OCT detection, to which optical AO-OCT systems are insensitive. Some computational AO approaches may also be highly sensitive to eye motion, and questions remain about whether computational AO is presently fast enough for real-time imaging, an important consideration for commercialization and clinical deployment. Finally, whatever computational AO's advantages turn out to be, it will have a lower SNR than comparable point scanning AO modalities because it captures less light, an effect visible in models of the AO-OCT transfer function.[121] In spite of these technical challenges, this continues to be an active and productive area of research.

Wavefront Sensorless AO-OCT

Wavefront sensorless AO-OCT[122] provides an interesting alternative to classical AO-OCT systems. In wavefront sensorless AO correction, the brightness or sharpness of imaged structures, rather than the aberrations measured by the wavefront sensor, are used to find the optimal shape of the wavefront corrector. This approach is particularly attractive for imaging patients who present challenges for standard AO imaging due to cataract or irregular pupil size or shape, and might open doors to compact low-cost AO-OCT systems. The disadvantage of existing sensorless approaches is that they typically require computationally costly optimization algorithms that reduce their bandwidth compared to typical sensor-based systems.

Prospects for Commercialization or Clinical Deployment of AO-OCT

The key technical factors limiting commercialization and clinical deployment of AO-OCT are cost, optical complexity, data volume, speed, and image postprocessing and analysis. The single most expensive component in most AO-OCT systems is the deformable mirror. Factoring in the cost of the mirror and the costs of the additional calibration equipment and software, the addition of AO to a clinical OCT system could easily double its cost.

A second factor is the optical complexity and size of AO-OCT systems. Due to the presence of the deformable mirror, and the attendant requirement that each scanner be conjugated to the pupil plane of the system, the imaging channel of AO-OCT systems tends to be long and to have many components. The size and complexity of the system requires frequent calibration and alignment, procedures that add cost to commercial systems.

Conventional OCT systems can afford to sample the retina at intervals of 10 to 15 μm, since denser sampling is not generally necessary without an associated improvement in lateral resolution. Adaptive optics OCT systems, by contrast, require the retina to be sampled more densely, every 1 to 2 μm. Thus in the case of volumetric imaging of a given retinal patch size, AO-OCT data sets are 100 times larger than their conventional OCT counterparts. Storage and accessibility of AO-OCT data already pose a challenge for investigators; widespread use of AO-OCT in the clinic would multiply this problem.

The benefits of AO are clearly visible in en face views of the retina, where the lateral resolution benefit is most apparent. Because AO-OCT is presently an order of magnitude slower than AO-SLO, eye movement artifacts in its images are significantly worse, and these are especially evident in en face views of the retina. Much progress is being made in mitigating these artifacts, through active eye tracking and postprocessing methods, but commercialization probably depends on either a significant increase in OCT speed or a definitive solution to mitigating eye movement artifacts.

Finally, effective commercialization depends on providing clinicians with flags or figures of merit that summarize the enormous amount of data in each image. Development of such summary figures is a likely outcome of current collaborations between clinicians and AO-OCT engineers and scientists, and these may improve the outlook for clinical use of the technology.

Because AO-OCT investigation of disease is still nascent, we do not yet know of a disease for which AO-OCT is required for effective treatment or management, but such a discovery might justify the added cost and complexity of AO-OCT in the future.

Investigative Ophthalmology & Visual Science

Conclusions

Adaptive optics OCT has produced a number of fundamental findings about the microstructure of the living human retina, and promises to grow in popularity as the complexity and cost of the required technology fall, while interest grows in the cellular and other microscopic constituents of retinal tissue, function, and dysfunction.

Acknowledgments

The authors thank Iwona Gorczynska, Susan Garcia, Justin Migacz, and Steve Jones for their technical and clinical assistance, as well as the National Institutes of Health (NIH) for Biomedical Research Partnership (BRP) Grant R01 EY014743, which provided indispensable funding for AO-OCT research between 2003 and 2012. This grant was a defining influence on the field, resulting in 75 publications in 26 journals from 10 lead author institutions, three patents, several subsequent NIH grants (R01 EY 024239 [JSW], R01 EY 018339 [DTM], K99 EY 026068 [RSJ]), and the training of dozens of graduate students and postdoctoral researchers.

Supported by grants from the National Institutes of Health (R01 EY 024239 [JSW], R01 EY 018339 [DTM], K99 EY 026068 [RSJ]) and an unrestricted grant from Research to Prevent Blindness, Incorporated.

Disclosure: **R.S. Jonnal**, P; **O.P. Kocaoglu**, None; **R.J. Zawadzki**, None; **Z. Liu**, None; **D.T. Miller**, P; **J.S. Werner**, None

References

1. Huang D, Swanson EA, Lin CP, et al. Optical coherence tomography. *Science*. 1991;254:1178–1181.
2. FitzGibbon T, Taylor S. Mean retinal ganglion cell axon diameter varies with location in the human retina. *Jpn J Ophthalmol*. 2012;56:631–637.
3. Sarks S, Arnold J, Killingsworth M, Sarks J. Early drusen formation in the normal and aging eye and their relation to age related maculopathy: a clinicopathological study. *Br J Ophthalmol*. 1999;83:358–368.
4. Yuodelis C, Hendrickson A. A qualitative and quantitative analysis of the human fovea during development. *Vision Res*. 1986;26:847–855.
5. Rodieck RW. *The First Steps in Seeing*. Sunderland, MA: Sinaur Associates; 1998.
6. Hendrickson A, Drucker D. The development of parafoveal and mid-peripheral human retina. *Behav Brain Res*. 1992;49:21–31.
7. Rosen R. *Optimality Principles in Biology*. New York: Springer; 2013.
8. Reichenbach A, Wolburg H. Astrocytes and ependymal glia. In: Kettenmann H, Ransom B, eds. *Neuroglia*. Oxford, New York: Oxford University Press, Inc.; 2005.
9. Curcio C, Sloan K, Kalina R, Hendrickson A. Human photoreceptor topography. *J Comp Neurol*. 1990;292:497–523.
10. Downey GP, Doherty DE, Schwab B, Elson E, Henson P, Worthen G. Retention of leukocytes in capillaries: role of cell size and deformability. *J Appl Physiol*. 1990;69:1767–1778.
11. Takayama K, Ooto S, Hangai M, et al. High-resolution imaging of the retinal nerve fiber layer in normal eyes using adaptive optics scanning laser ophthalmoscopy. *PLoS One*. 2012;7:e33158.
12. Kocaoglu OP, Cense B, Jonnal RS, et al. Imaging retinal nerve fiber bundles using optical coherence tomography with adaptive optics. *Vision Res*. 2011;51:1835–1844.
13. Choi W, Mohler KJ, Potsaid B, et al. Choriocapillaris and choroidal microvasculature imaging with ultrahigh speed OCT angiography. *PLoS One*. 2013;12:e81499.
14. Braaf B, Vienola KV, Sheehy CK, et al. Real-time eye motion correction in phase-resolved OCT angiography with tracking SLO. *Biomed Opt Express*. 2013;4:51–65.
15. Mayer E, Carter D, Ren Y, et al. Neural progenitor cells from postmortem adult human retina. *Br J Ophthalmol*. 2005;89:102–106.
16. Harman A, Abrahams B, Moore S, Hoskins R. Neuronal density in the human retinal ganglion cell layer from 16–77 years. *Anat Rec*. 2000;260:124–131.
17. Crooks J, Kolb H. Localization of gABA, glycine, glutamate and tyrosine hydroxylase in the human retina. *J Comp Neurol*. 1992;315:287–302.
18. Humayun MS, de Juan E Jr, Weiland JD, et al. Pattern electrical stimulation of the human retina. *Vision Res*. 1999;39:2569–2576.
19. Morgan JI, Dubra A, Wolfe R, Merigan WH, Williams DR. In vivo autofluorescence imaging of the human and macaque retinal pigment epithelial cell mosaic. *Invest Ophthalmol Vis Sci*. 2009;50:1350–1359.
20. Friberg TR, Brennen PM. Analysis of the relationship between drusen size and drusen area in eyes with age-related macular degeneration. *Ophthalmic Surg Lasers Imaging Retina*. 2011;42:369.
21. Kolb H, Linberg KA, Fisher SK. Neurons of the human retina: a golgi study. *J Comp Neurol*. 1992;318:147–187.
22. Moore J, Bagley S, Ireland G, McLeod D, Boulton M. Three dimensional analysis of microaneurysms in the human diabetic retina. *J Anat*. 1999;194:89–100.
23. Dubow M, Pinhas A, Shah N, et al. Classification of human retinal microaneurysms using adaptive optics scanning light ophthalmoscope fluorescein angiography. *Invest Ophthalmol Vis Sci*. 2014;55:1299–1309.
24. Wong TY, Klein R, Klein BE, Meuer SM, Hubbard LD. Retinal vessel diameters and their associations with age and blood pressure. *Invest Ophthalmol Vis Sci*. 2003;44:4644–4650.
25. Polyak S. *The Retina*. Chicago: University of Chicago Press; 1941.
26. Tasman W, Jaeger EA. *Duane's Ophthalmology, 2009 Edition*. Philadelphia, PA: Lippincott Williams & Wilkins; 2013.
27. Thibos L, Hong X, Bradley A, Cheng X. Statistical variation of aberration structure and image quality in a normal population of healthy eyes. *J Opt Soc Am A*. 2002;19:2329–2348.
28. Doble N, Miller DT, Yoon G, Williams DR. Requirements for discrete actuator and segmented wavefront correctors for aberration compensation in two large populations of human eyes. *Appl Optics*. 2007;46:4501–4514.
29. Liang J, Williams DR, Miller DT. Supernormal vision and high-resolution retinal imaging through adaptive optics. *J Opt Soc Am A*. 1997;14:2884–2892.
30. Hofer H, Artal P, Singer B, Aragón JL, Williams DR. Dynamics of the eye's wave aberration. *J Opt Soc Am A*. 2001;18:497–506.
31. Diaz-Santana L, Torti C, Munro I, Gasson P, Dainty C. Benefit of higher closed-loop bandwidths in ocular adaptive optics. *Opt Express*. 2003;11:2597–2605.
32. Mira-Agudelo A, Lundström L, Artal P. Temporal dynamics of ocular aberrations: monocular vs binocular vision. *Ophthalmic Physiol Opt*. 2009;29:256–263.
33. Yu Y, Zhang T, Meadway A, Wang X, Zhang Y. High-speed adaptive optics for imaging of the living human eye. *Opt Express*. 2015;23:23035–23052.
34. Nirmaier T, Pudasaini G, Bille J. Very fast wave-front measurements at the human eye with a custom CMOS-based Hartmann-Shack sensor. *Opt Express*. 2003;11:2704–2716.
35. Cense B, Gao W, Brown JM, et al. Retinal imaging with polarization-sensitive optical coherence tomography and adaptive optics. *Opt Express*. 2009;17:21634–21651.

Investigative Ophthalmology & Visual Science

36. Kocaoglu OP, Lee S, Jonnal RS, et al. Imaging cone photoreceptors in three dimensions and in time using ultrahigh resolution optical coherence tomography with adaptive optics. *Biomed Opt Express*. 2011;2:748–763.
37. Williams D. Imaging single cells in the living retina. *Vision Res*. 2011;51:1379–1396.
38. Carroll J, Kay DB, Scoles D, Dubra A, Lombardo M. Adaptive optics retinal imaging–clinical opportunities and challenges. *Curr Eye Res*. 2013;38:709–721.
39. Miller DT, Qu J, Jonnal RS, Thorn KE. Coherence gating and adaptive optics in the eye. *Proc SPIE*. 2003;4956:65.
40. Hermann B, Fernandez E, Unterhuber A, et al. Adaptive-optics ultrahigh-resolution optical coherence tomography. *Opt Lett*. 2004;29:2142–2144.
41. Fernández EJ, Považay B, Hermann B, et al. Three-dimensional adaptive optics ultrahigh-resolution optical coherence tomography using a liquid crystal spatial light modulator. *Vision Res*. 2005;45:3432–3444.
42. Fercher AF, Hitzenberger CK, Kamp G, El-Zaiat SY. Measurement of intraocular distances by backscattering spectral interferometry. *Opt Commun*. 1995;117:43–48.
43. Zhang Y, Rha J, Jonnal RS, Miller DT. Adaptive optics parallel spectral domain optical coherence tomography for imaging the living retina. *Opt Express*. 2005;13:4792–4811.
44. Zawadzki R, Jones S, Olivier S, et al. Adaptive-optics optical coherence tomography for high-resolution and high-speed 3D retinal in vivo imaging. *Opt Express*. 2005;13:8532–8546.
45. Zhang Y, Cense B, Rha J, et al. High-speed volumetric imaging of cone photoreceptors with adaptive optics spectral-domain optical coherence tomography. *Opt Express*. 2006;14:4380–4394.
46. Zawadzki RJ, Cense B, Zhang Y, Choi SS, Miller DT, Werner JS. Ultrahigh-resolution optical coherence tomography with monochromatic and chromatic aberration correction. *Opt Express*. 2008;16:8126–8143.
47. Fernández EJ, Hermann B, Považay B, et al. Ultrahigh resolution optical coherence tomography and pancorrection for cellular imaging of the living human retina. *Opt Express*. 2008;16:11083–11094.
48. Jones S, Olivier S, Chen D, et al. Adaptive optics ophthalmologic systems using dual deformable mirrors. In: *MOEMS-MEMS 2007 Micro and Nanofabrication. International Society for Optics; Photonics*. 2007;64670H–64670H.
49. Zawadzki RJ, Choi SS, Jones SM, Oliver SS, Werner JS. Adaptive optics-optical coherence tomography: optimizing visualization of microscopic retinal structures in three dimensions. *J Opt Soc Am A*. 2007;24:1373–1383.
50. Evans JW, Zawadzki RJ, Jones SM, Olivier SS, Werner JS. Error budget analysis for an adaptive optics optical coherence tomography system. *Opt Express*. 2009;17:13768–13784.
51. Mujat M, Ferguson RD, Patel AH, Iftimia N, Lue N, Hammer DX. High resolution multimodal clinical ophthalmic imaging system. *Opt Express*. 2010;18:11607–11621.
52. Ferguson RD, Zhong Z, Hammer DX, et al. Adaptive optics scanning laser ophthalmoscope with integrated wide-field retinal imaging and tracking. *J Opt Soc Am A*. 2010;27:A265–A277.
53. Dubra A, Sulai Y. Reflective afocal broadband adaptive optics scanning ophthalmoscope. *Biomed Opt Express*. 2011;2:1757–1768.
54. Lee S-H, Werner JS, Zawadzki RJ. Improved visualization of outer retinal morphology with aberration cancelling reflective optical design for adaptive optics-optical coherence tomography. *Biomed Opt Express*. 2013;4:2508–2517.
55. Liu Z, Kocaoglu OP, Miller DT. In-the-plane design of an off-axis ophthalmic adaptive optics system using toroidal mirrors. *Biomed Opt Express*. 2013;4:3007–3029.
56. Torti C, Považay B, Hofer B, et al. Adaptive optics optical coherence tomography at 120,000 depth scans/s for non-invasive cellular phenotyping of the living human retina. *Opt Express*. 2009;17:19382–19400.
57. Kocaoglu OP, Ferguson RD, Jonnal RS, et al. Adaptive optics optical coherence tomography with dynamic retinal tracking. *Biomed Opt Express*. 2014;5:2262–2284.
58. Pircher M, Zawadzki R, Evans J, Werner J, Hitzenberger C. Simultaneous imaging of human cone mosaic with adaptive optics enhanced scanning laser ophthalmoscopy and high-speed transversal scanning optical coherence tomography. *Opt Lett*. 2008;33:22–24.
59. Kocaoglu OP, Turner TL, Liu Z, Miller DT. Adaptive optics optical coherence tomography at 1 MHz. *Biomed Opt Express*. 2014;5:4186–4200.
60. Merino D, Dainty C, Bradu A, Podoleanu AG. Adaptive optics enhanced simultaneous en-face optical coherence tomography and scanning laser ophthalmoscopy. *Opt Express*. 2006;14:3345–3353.
61. Zawadzki RJ, Jones SM, Pilli S, et al. Integrated adaptive optics optical coherence tomography and adaptive optics scanning laser ophthalmoscope system for simultaneous cellular resolution in vivo retinal imaging. *Biomed Opt Express*. 2011;2:1674–1686.
62. Meadway A, Girkin CA, Zhang Y. A dual-modal retinal imaging system with adaptive optics. *Opt Express*. 2013;21:29792–29807.
63. Zawadzki RJ, Capps AG, Kim DY, et al. Progress on developing adaptive optics–optical coherence tomography for in vivo retinal imaging: monitoring and correction of eye motion artifacts. *IEEE Sel Top Quantum Electron*. 2014;20:322–333.
64. Fuller AR, Zawadzki RJ, Choi S, Wiley DF, Werner JS, Hamann B. Segmentation of three-dimensional retinal image data. *IEEE Trans Vis Comput Graph*. 2007;13:1719–1726.
65. Zawadzki RJ, Fuller AR, Wiley DF, Hamann B, Choi SS, Werner JS. Adaptation of a support vector machine algorithm for segmentation and visualization of retinal structures in volumetric optical coherence tomography data sets. *J Biomed Opt*. 2007;12:041206.
66. Garvin MK, Abràmoff MD, Kardon R, Russell SR, Wu X, Sonka M. Intraretinal layer segmentation of macular optical coherence tomography images using optimal 3-d graph search. *IEEE Trans Med Imaging*. 2008;27:1495–1505.
67. Garvin MK, Abràmoff MD, Wu X, Russell SR, Burns TL, Sonka M. Automated 3-d intraretinal layer segmentation of macular spectral-domain optical coherence tomography images. *IEEE Trans Med Imaging*. 2009;28:1436–1447.
68. Chiu SJ, Li XT, Nicholas P, Toth CA, Izatt JA, Farsiu S. Automatic segmentation of seven retinal layers in SDOCT images congruent with expert manual segmentation. *Opt Express*. 2010;18:19413–19428.
69. Chiu SJ, Izatt JA, O'Connell RV, Winter KP, Toth CA, Farsiu S. Validated automatic segmentation of AMD pathology including drusen and geographic atrophy in SD-OCT images. *Invest Ophthalmol Vis Sci*. 2012;53:53–61.
70. Srinivasan VJ, Monson BK, Wojtkowski M, et al. Characterization of outer retinal morphology with high-speed, ultrahigh-resolution optical coherence tomography. *Invest Ophthalmol Vis Sci*. 2008;49:1571–1579.
71. Fabritius T, Makita S, Miura M, Myllylä R, Yasuno Y. Automated segmentation of the macula by optical coherence tomography. *Opt Express*. 2009;17:15659–15669.
72. Mishra A, Wong A, Bizheva K, Clausi DA. Intra-retinal layer segmentation in optical coherence tomography images. *Opt Express*. 2009;17:23719–23728.
73. Götzinger E, Pircher M, Geitzenauer W, et al. Retinal pigment epithelium segmentation by polarization sensitive optical coherence tomography. *Opt Express*. 2008;16:16410–16422.
74. Cense B, Koperda E, Brown JM, et al. Volumetric retinal imaging with ultrahigh-resolution spectral-domain optical

Investigative Ophthalmology & Visual Science

coherence tomography and adaptive optics using two broadband light sources. *Opt Express*. 2009;17:4095–4111.

75. Jonnal RS, Kocaoglu OP, Zawadzki RJ, Lee S-H, Werner JS, Miller DT. The cellular origins of the outer retinal bands in optical coherence tomography images. *Invest Ophthalmol Vis Sci*. 2014;55:7904–7918.
76. Jonnal RS, Kocaoglu OP, Zawadzki RJ, Lee S-H, Werner JS, Miller DT. Author response: outer retinal bands. *Invest Ophthalmol Vis Sci*. 2015;56:2507–2510.
77. Jonnal RS, Kocaoglu OP, Wang Q, Lee S, Miller DT. Phase-sensitive imaging of the outer retina using optical coherence tomography and adaptive optics. *Biomed Opt Express*. 2012; 3:104–124.
78. Zawadzki RJ, Choi SS, Fuller AR, Evans JW, Hamann B, Werner JS. Cellular resolution volumetric in vivo retinal imaging with adaptive optics–optical coherence tomography. *Opt Express*. 2009;17:4084–4094.
79. Stevenson S. Eye movement recording and retinal image stabilization with high magnification retinal imaging. *J Vis*. 2006;6(13):39.
80. Pircher M, Kroisamer J, Felberer F, Sattmann H, Götzinger E, Hitzenberger C. Temporal changes of human cone photoreceptors observed in vivo with SLO/OCT. *Biomed Opt Express*. 2011;2:100–112.
81. Choma MA, Ellerbee AK, Yang C, Creazzo TL, Izatt JA. Spectral-domain phase microscopy. *Opt Lett*. 2005;30:1162–1164.
82. Spaide RF, Curcio CA. Anatomical correlates to the bands seen in the outer retina by optical coherence tomography: literature review and model. *Retina*. 2011;31:1609–1619.
83. Staurenghi G, Sadda S, Chakravarthy U, Spaide RF. Proposed lexicon for anatomic landmarks in normal posterior segment spectral-domain optical coherence tomography: the IN·OCT consensus. *Ophthalmology*. 2014;121(8):1572–1578.
84. Spaide RF. Outer retinal bands. *Invest Ophthalmol Vis Sci*. 2015;56:2505–2506.
85. Jonnal RS, Besecker JR, Derby JC, et al. Imaging outer segment renewal in living human cone photoreceptors. *Opt Express*. 2010;18:5257–5270.
86. Liu Z, Kocaoglu OP, Turner TL, Miller DT. Modal content of living human cone photoreceptors. *Biomed Opt Express*. 2015;6:3378–3404.
87. Panorgias A, Zawadzki RJ, Capps AG, Hunter AA, Morse LS, Werner JS. Multimodal assessment of microscopic morphology and retinal function in patients with geographic atrophy. *Invest Ophthalmol Vis Sci*. 2013;54(6):4372–4384.
88. Wang Q, Tuten WS, Lujan BJ, et al. Adaptive optics microperimetry and OCT images show preserved function and recovery of cone visibility in macular telangiectasia type 2 retinal lesions. *Invest Ophthalmol Vis Sci*. 2015;56:778–786.
89. Zhang Y, Wang X, Rivero EB, et al. Photoreceptor perturbation around subretinal drusenoid deposits as revealed by adaptive optics scanning laser ophthalmoscopy. *Am J Ophthalmol*. 2014;158:584–596.
90. Panda S, Jonas JB. Decreased photoreceptor count in human eyes with secondary angle-closure glaucoma. *Invest Ophthalmol Vis Sci*. 1992;33:2532–2536.
91. Kendell KR, Quigley HA, Kerrigan LA, Pease ME, Quigley EN. Primary open-angle glaucoma is not associated with photoreceptor loss. *Invest Ophthalmol Vis Sci*. 1995;36:200–205.
92. Nork TM, Ver Hoeve JN, Poulsen GL, et al. Swelling and loss of photoreceptors in chronic human and experimental glaucomas. *Arch Ophthalmol*. 2000;118:235–245.
93. Choi SS, Zawadzki RJ, Lim MC, et al. Evidence of outer retinal changes in glaucoma patients as revealed by ultrahigh-resolution in vivo retinal imaging. *Br J Ophthalmol*. 2010; 131–141.
94. Werner J, Keltner J, Zawadzki R, Choi S. Outer retinal abnormalities associated with inner retinal pathology in nonglaucomatous and glaucomatous optic neuropathies. *Eye*. 2011;25:279–289.
95. De Boer JF, Milner TE, van Gemert MJ, Nelson JS. Two-dimensional birefringence imaging in biological tissue by polarization-sensitive optical coherence tomography. *Opt Lett*. 1997;22:934–936.
96. Nadler Z, Wang B, Schuman JS, et al. In vivo three-dimensional characterization of the healthy human lamina cribrosa with adaptive optics spectral-domain optical coherence tomography. *Invest Ophthalmol Vis Sci*. 2014;55:6459–6466.
97. Kim DY, Werner JS, Zawadzki RJ. Complex conjugate artifact-free adaptive optics optical coherence tomography of in vivo human optic nerve head. *J Biomed Opt*. 2012;12:126005.
98. Lombardo M, Parravano M, Serrao S, Ducoli P, Stirpe M, Lombardo G. Analysis of retinal capillaries in patients with type 1 diabetes and nonproliferative diabetic retinopathy using adaptive optics imaging. *Retina*. 2013;33:1630–1639.
99. Wang Q, Kocaoglu OP, Cense B, et al. Imaging retinal capillaries using ultrahigh-resolution optical coherence tomography and adaptive optics. *Invest Ophthalmol Vis Sci*. 2011;52:6292–6299.
100. Kurokawa K, Sasaki K, Makita S, Hong Y-J, Yasuno Y. Three-dimensional retinal and choroidal capillary imaging by power Doppler optical coherence angiography with adaptive optics. *Opt Express*. 2012;20:22796–22812.
101. Felberer F, Rechenmacher M, Haindl R, Baumann B, Hitzenberger CK, Pircher M. Imaging of retinal vasculature using adaptive optics SLO/OCT. *Biomed Opt Express*. 2015; 6:1407–1418.
102. Park SS, Bauer G, Abedi M, et al. Intravitreal autologous bone marrow cD34+ cell therapy for ischemic and degenerative retinal disorders: preliminary phase 1 clinical trial findings. *Invest Ophthalmol Vis Sci*. 2014;56(1):81–89.
103. Bizheva K, Pflug R, Hermann B, et al. Optophysiology: depth-resolved probing of retinal physiology with functional ultrahigh-resolution optical coherence tomography. *Proc Natl Acad Sci U S A*. 2006;103:5066–5071.
104. Srinivasan VJ, Wojtkowski M, Fujimoto JG, Duker JS. In vivo measurement of retinal physiology with high-speed ultrahigh-resolution optical coherence tomography. *Opt Lett*. 2006;31: 2308–2310.
105. Srinivasan V, Chen Y, Duker J, Fujimoto J. In vivo functional imaging of intrinsic scattering changes in the human retina with high-speed ultrahigh resolution OCT. *Opt Express*. 2009; 17:3861–3877.
106. Grieve K, Roorda A. Intrinsic signals from human cone photoreceptors. *Invest Ophthalmol Vis Sci*. 2008;49:713–719.
107. Jonnal RS, Rha J, Zhang Y, Cense B, Gao W, Miller DT. In vivo functional imaging of human cone photoreceptors. *Opt Express*. 2007;15:16141–16160.
108. Liu Z, Kocaoglu OP, Turner TL, Miller DT. Imaging human retinal pigment epithelium cells using adaptive optics optical coherence tomography. *Proc SPIE*. 2016;96931E.
109. Chen J, Saeki F, Wiley BJ, et al. Gold nanocages: bioconjugation and their potential use as optical imaging contrast agents. *Nano Lett*. 2005;5:473–477.
110. Lee TM, Oldenburg AL, Sitafalwalla S, et al. Engineered microsphere contrast agents for optical coherence tomography. *Opt Lett*. 2003;28:1546–1548.
111. Rao KD, Choma MA, Yazdanfar S, Rollins AM, Izatt JA. Molecular contrast in optical coherence tomography by use of a pump probe technique. *Opt Lett*. 2003;28:340–342.
112. Paranjape AS, Kuranov R, Baranov S, et al. Depth resolved photothermal OCT detection of macrophages in tissue using nanorose. *Biomed Opt Express*. 2010;1:2–16.

Investigative Ophthalmology & Visual Science

113. Kim S, Rinehart MT, Park H, Zhu Y, Wax A. Phase-sensitive OCT imaging of multiple nanoparticle species using spectrally multiplexed single pulse photothermal excitation. *Biomed Opt Express*. 2012;3:2579–2586.
114. Gorczynska I, Migacz JV, Zawadzki RJ, Capps AG, Werner JS. Comparison of amplitude-decorrelation, speckle-variance and phase-variance OCT angiography methods for imaging the human retina and choroid. *Biomed Opt Express*. 2016;7:911–942.
115. O'Connor NJ, Bartsch D-U, Freeman WJ, Mueller AJ, Holmes TJ. Fluorescent infrared scanning-laser ophthalmoscope for three-dimensional visualization: automatic random-eye-motion correction and deconvolution. *Appl Optics*. 1998;37:2021–2033.
116. Christou JC, Roorda A, Williams DR. Deconvolution of adaptive optics retinal images. *J Opt Soc Am A*. 2004;21:1393–1401.
117. Iglesias I, Artal P. High-resolution retinal images obtained by deconvolution from wave-front sensing. *Opt Lett*. 2000;25:1804–1806.
118. Catlin D, Dainty C. High-resolution imaging of the human retina with a Fourier deconvolution technique. *J Opt Soc Am A*. 2002;19:1515–1523.
119. Shemonski ND, South FA, Liu Y-Z, Adie SG, Carney PS, Boppart SA. Computational high-resolution optical imaging of the living human retina. *Nat Photonics*. 2015;9:440–443.
120. Kumar A, Kamali T, Platzer R, Unterhuber A, Drexler W, Leitgeb RA. Anisotropic aberration correction using region of interest based digital adaptive optics in Fourier domain OCT. *Biomed Opt Express*. 2015;6:1124–1134.
121. Verstraete HR, Cense B, Bilderbeek R, Verhaegen M, Kalkman J. Towards model-based adaptive optics optical coherence tomography. *Opt Express*. 2014;22:32406–32418.
122. Jian Y, Xu J, Gradowski MA, Bonora S, Zawadzki RJ, Sarunic MV. Wavefront sensorless adaptive optics optical coherence tomography for in vivo retinal imaging in mice. *Biomed Opt Express*. 2014;5:547–559.

Investigative Ophthalmology & Visual Science